

The Honda Automotive Laboratories of Ohio Wind Tunnel

Scott Best, Ghazi Bari, Tyler Brooker, Guy Flynt, Joel Walter, and Ed Duell Jacobs

Abstract

The Honda Automotive Laboratories of Ohio (HALO) includes a new aeroacoustic wind tunnel located near Marysville, Ohio that started operations in 2022. This facility provides world-class aerodynamic flow quality and acoustic testing capabilities for the development of both passenger and motorsports vehicles.

This closed-return $\frac{3}{4}$ open jet wind tunnel features a two-position flexible nozzle system with cross sections of 25 m² and 18 m², providing wind speeds of up to 250 km/h and 310 km/h, respectively. There is a ± 180 degree turntable with boundary layer control systems, and interchangeable single belt and 5-belt moving ground plane (MGP) modules. Extensive applications of acoustic treatment in the test section and throughout the wind tunnel circuit provide a hemi-anechoic test environment and low background noise levels. A temperature control system provides uniform and stable air temperature over an operating environment between 10 °C and 50 °C.

The primary instrumentation of the wind tunnel includes the wind speed, temperature, and humidity measurement systems, a 6-component force balance integrated within the turntable, and an acoustic test system (ATS). The ATS includes four planar microphone arrays for external measurements and a spherical microphone array and binaural heads for internal measurements. A flow survey traverse system equipped with a 4-D probe holder mechanism is capable of placing a probe anywhere within the test volume.

The HALO facility includes the wind tunnel control room, secure vehicle preparation bays and office spaces for segregated customers, and a vehicle frontal and side area measurement system.

This paper provides an introduction to the HALO wind tunnel testing capabilities, design features and development, and the results of the aeroacoustic commissioning program. The background noise level and flow quality characteristics are provided.

Introduction

Honda began operation of its new aeroacoustic wind tunnel in 2022, as part of the Honda Automotive Laboratories of Ohio (HALO) located at the Transportation Research Center, Inc.. Jacobs was the wind tunnel designer and also managed procurement, construction, installation, and facility commissioning, and held responsibility for the technical performance of the wind tunnel and integrated test systems.

HALO provides Honda Development and Manufacturing of America, LLC with testing capability to support the development of vehicle

products designed and built in America. These development efforts include continued improvements in passenger vehicle fuel economy and driving dynamics as well as reductions in wind and road noise intrusion.

The HALO wind tunnel provides three testing functions in one facility: passenger vehicle aerodynamics, passenger vehicle aeroacoustics, and motorsports aerodynamics. The wind tunnel test section is reconfigurable for each of these roles, with a two-position flex nozzle, interchangeable moving ground plane systems, and rapidly-deployable measurement equipment including a flow survey traverse and microphone phased arrays.

Passenger vehicle aerodynamics testing focuses on the study of forces acting on the vehicle. Drag force has a direct impact on the fuel economy or travel range of vehicles with internal combustion engines and electric drives, respectively. This testing is accomplished with the large 25 m² nozzle and 5-belt moving ground plane (MGP) system, and with the support of a flow survey traverse system that can place an air data probe anywhere within the test volume. This configuration offers the greatest air flow simulation quality and most direct coupling between the vehicle and six-component force balance.

Passenger vehicle acoustic testing focuses on the study of wind noise generated by a vehicle and the transmission of noises into the passenger cabin. This testing is accomplished with the large nozzle, with boundary layer systems closed off, and with microphone arrays and other acoustic sensors deployed both surrounding the vehicle and within the cabin interior. A moving ground plane cover can be installed to provide a minimum background noise level.

Motorsports aerodynamics testing focuses on the forces acting on racing vehicles, and this is accomplished with the small 18 m² nozzle and single belt MGP. This configuration provides the high wind speed and underbody flow fidelity necessary for accurate simulation of vehicles with very low ground clearance and high-downforce features such as spoilers.

This paper presents the HALO wind tunnel performance and measurement capabilities, the key design features of the facility, some critical wind tunnel design development efforts, and the aeroacoustic acceptance testing results which characterize the quality of the aerodynamic and acoustic simulation provided.

Wind Tunnel Test Capabilities

This section provides a high-level description of the wind tunnel circuit as background information, and then focuses on the key capabilities that the wind tunnel offers to users as a test laboratory. More detailed descriptions of the wind tunnel features are discussed in the Wind Tunnel Key Features section.

Performance Capabilities

The HALO wind tunnel is a closed-return circuit with a $\frac{3}{4}$ open jet test section. Figure 1 shows a plan view of the wind tunnel, with some of the major components highlighted. The test section features a two-position nozzle which changes between 25 m² and 18 m² exit area at the operator's command. The test section includes a 12.5 m diameter turntable, which houses a force balance and an interchangeable 5-belt or single belt moving ground plane (MGP) module. The jet length is 15.2 m before the flow is directed by the collector into the high speed diffuser. Flow proceeds through Corners 1 and 2 to the main fan, which is located in the return leg. The backleg diffuser expands the flow towards Corner 3, and Corner 4 directs the flow through the stilling chamber and into the contraction. The overall airline footprint (excluding resonators) is 94.4 m by 41.6 m.

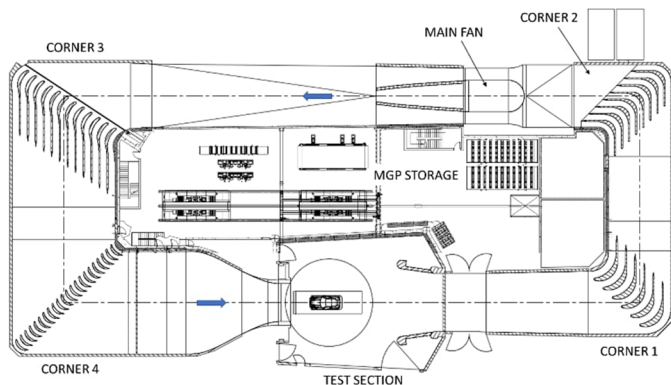


Figure 1. The HALO wind tunnel general arrangement plan view.

The maximum wind speeds simulated in the wind tunnel are 250 km/h with the 25 m² nozzle and 310 km/h with the 18 m² nozzle. The 5-belt MGP can operate up to 270 km/h and the single belt MGP can operate up to 310 km/h. Acceleration and deceleration between 10 km/h and top speed is achieved in under 60 seconds. The wind tunnel is seen configured for motorsports testing with the small nozzle and single belt MGP in Figure 2.

The boundary layer removal systems (BLRS) operate to provide uniform flow above the MGPs, and in particular uniform boundary layer shape across the width of the single belt. These systems were designed to produce minimal impact to static pressure distribution and flow angularity.

The wind tunnel features temperature and humidity control, with a heat exchanger and steam injection located in Corner 3, and dry conditioned air supplied to the balance room and from there into the test section. Air temperature is held within a standard deviation of less than 1 °C from setpoint with an operating envelope from 10 °C to 50 °C. Humidity is regulated to a maximum 12 °C dew point, with a control band of +/- 1 °C dew point.



Figure 2. Motorsports testing up to 310 km/h is performed with the small nozzle and single belt moving ground plane.

The wind tunnel and test section feature extensive treatments with acoustically-absorbent materials. The test section is ISO 3745 certified as a hemi-anechoic free-field test environment between 50 Hz and 20 kHz, and the background noise levels in acoustic testing configuration are under 48 dB(A), 57 dB(A), and 61 dB(A) at 100 km/h, 140 km/h, and 160 km/h, respectively.

The HALO wind tunnel generates minimal low-frequency pulsation, with $C_{PRMS} < 0.45\%$ within the frequency band $0.5 \text{ Hz} \leq f \leq 20 \text{ Hz}$ between 80 km/h and maximum wind speed.

Details about the aerodynamic, acoustic, and climate performance as measured during facility commissioning are provided in the Aeroacoustic Acceptance Testing and Results section.

Measurement Systems

The primary purpose of any laboratory is data collection, and so the HALO wind tunnel has several measurement systems, including acoustic test systems, a 6-component force balance, and a flow survey traverse for positioning probes at any point of interest in the flow. Facility process measurement systems are used to control and record the conditions simulated by the wind tunnel.

Acoustic Test Systems

The acoustic test systems were supplied by Siemens AG and centers around four external planar arrays, a cabin interior spherical array, and biaural heads connected to a multi-channel conditioning amplifier and data acquisition system. The planar arrays consist of two 6 m diameter semi-circular side arrays, a 6 m diameter circular overhead array, and 2.1 m diameter circular front array, as can be seen in Figure 3. The array support structures provide positioning repeatability of 1.5 mm and maximum deflection under wind load of 1.5 mm, as necessary for the accurate functioning of the arrays.

The microphone arrays enable rapid location of noise sources from the test object interaction with wind, such as at the side mirrors, wheel wells, or front grille. The arrangement of the arrays around the vehicle allows for mapping of these noise sources on all critical areas. The performance of the acoustic arrays is defined by dynamic range and spatial resolution and is summarized in Table 1. The numbers of microphones used for the arrays are 120 per side array, 167 for the overhead array, and 95 for the front array. Each array includes a central camera to capture images for noise map graphical overlay.



Figure 3. The test section configured for acoustic testing with exterior microphone arrays deployed.

Table 1. Microphone array dynamic range and spatial resolution

f (Hz)	Dynamic Range (dB)			Spatial Resolution (mm)		
	Sides	OH	Front	Sides	OH	Front
500	21.5	17.0	17.0	560	700	1810
1000	20.8	19.9	19.9	300	360	880
2000	16.6	16.7	16.7	150	170	420
4000	14.9	14.8	16.7	80	90	200
8000	15.3	15.1	17.1	40	50	90
16,000	14.8	15.8	17.5	20	30	50

Selected frequency bands can be processed and displayed on a console in the wind tunnel control room in real time, providing an overlay “heat map” of noise over a video camera image of the test object, such as shown in Figure 4. Post-processing for detailed review and documentation is performed on additional consoles located in secure office spaces.



Figure 4. Broad-spectrum noise map image generated by the acoustic test system for a mass production SUV at yawed at 30 degrees with a 100 km/h wind.

A spherical array with 54 microphones is used to locate noise sources from within the vehicle interior and operates with the same principles

as the exterior planar arrays. Biaural heads are used to allow replication of the human ear’s perception of noise within the vehicle cabin via earphones worn by the test engineer.

The acoustic test system has a total of 616 audio input channels, which includes the addition of discrete free-field or surface-mount microphones for noise level analysis and recording. 24 of these channels are located in the flow survey traverse so that microphones may be located nearly anywhere within the test section volume.

6-Component Force Balance

The turntable, moving ground plane (MGP) systems, and force balance were supplied by MTS Systems. The 6-component force balance is integrated into the turntable and operates with both the 5-belt and single belt MGP modules. Descriptions of the moving ground plane systems and balance connections are provided in the Wind Tunnel Key Features section.

The MGP and balance have capacity for vehicles up to 4800 kg, with wheelbase between 1850 mm and 4400 mm and track width between 1480 mm and 2210 mm. The balance calibrated ranges and static error band accuracy specifications are listed in Table 2.

Table 2. Balance ranges and accuracy

	min	max	accuracy
Fx	-500 N	6000 N	0.9 N
Fy	-6500 N	6500 N	0.9 N
Fz	-6000 N	6000 N	1.4 N
Mx	-6500 N-m	6500 N-m	1.9 N-m
My	-6500 N-m	6500 N-m	1.9 N-m
Mz	-6500 N-m	6500 N-m	1.9 N-m

Flow Survey Traverse

The test section houses a flow survey traverse, which is used to position a probe or sensor anywhere within the test volume. Jacobs performed the design of the flow survey traverse system in-house. The traverse consists of an “X-beam”, which is aligned with the test section longitudinal axis and is suspended from the ceiling by two rails that run in the lateral (“Y”) direction. An “X-carriage” is attached to one side of the X-beam and moves fore and aft. A “Z-carriage” is attached to the X-carriage and moves vertically. A rigid strut is attached to the Z-carriage, and thus the base of this strut has the three translational degrees of freedom. The operational travel range of the traverse includes approximately 11 m in the X and Y axes and 5 m in the Z axis including the capability to take measurements 2 mm from the floor level.

The traverse includes X and Y axis maximum speeds of 300 mm/s, and 200 m/s for the Z axis to maximize test efficiency. The performance of the traverse is defined as the operational accuracy, repeatability, and deflection at the probe interface. The traverse position stopping accuracy is ± 0.5 mm and ± 1 mm while moving along a programmed path. The traverse positioning repeatability is less than 0.2 mm.

The traverse was designed for high stiffness under wind load conditions. Worst-case deflection is 0.5 mm with up to 900 N drag load or 300 N side load.

A 4D probe holder may be attached to the base of the traverse strut, and this provides additional degrees of freedom including roll, yaw, and pitch. Thus, a probe held by this mechanism can be placed anywhere within the flow volume and at a wide range of incidence to the flow. Figure 5 shows a probe held by the 4D probe holder in the wake region downstream of a vehicle in the test section.



Figure 5. The flow survey traverse positions a probe in the wake of a vehicle in the test section.

The flow survey traverse control system includes an integrated safety system with feature for personnel safety, maintenance mode, fault detection and collision avoidance to prevent contact with the test article, the collector, the nozzle, or the floor or walls of the test section.

Facility Measurement Systems

The wind tunnel facility measurement systems monitor wind speed, MGP speed, air temperature, and humidity, as well as all other test-relevant parameters including BLRS flow rates, turntable yaw angle, and flow survey traverse position.

The primary instruments for measuring air speed are pressure sensors, as well as humidity and temperature probes. Calibration for wind speed was performed for “nozzle method” and “plenum method” using a pitot-static probe at a reference location in the test volume. The nozzle method calibration maps the pitot-static probe measurements onto the pressure difference between static pressure taps in the stilling chamber and near the nozzle outlet. The pressure taps near the nozzle outlet are positioned at a location to capture approximately 80% of the pressure drop through the contraction. This placement is done to minimize vehicle blockage influence on the air speed value calculated via nozzle method.

The plenum method calibration maps the pitot-static probe measurements onto the pressure difference between pressure taps in the stilling chamber and a pressure tap in the overhead microphone array storage room. This storage room has large openings to the test section, but this measurement location is less subject to large-scale turbulent effects generated by the interaction of the $\frac{3}{4}$ open jet and the surrounding air within the test section.

The wind tunnel control system is programmed to use the Mercker airspeed calculation method if this is selected by the operator. Details of the Mercker method are available in [1].

Supporting Features

Wind tunnel operations are enabled and supported by control systems, test sequencing, data management, vehicle preparation spaces, and office facilities located within the support building. The wind tunnel operators, test engineers, and technicians overseeing a test reside in a spacious control room that features a 9.1 m wide by 1.8 m tall window for unimpeded visual access to the test section. There is also an observation room on the second floor of the support building, above the control room, with a viewing window into the test section. The control room and observation room windows have retractable acoustically-treated covers that can be deployed to minimize noise reflections within the test section for acoustic testing or for test privacy.

Client confidentiality was designed into the data management via a Test Cell Network and the support building architecture. Client access throughout the facility and within the computing network is managed for the confidentiality of the test articles and test data. There are separate access paths between vehicle prep bays on the first floor and client office spaces on the second floor, as well.

Wind Tunnel Key Features

The HALO wind tunnel design incorporates many features that work together to solve the multi-dimensional challenges associated with achieving the performance characteristics necessary to provide the testing capabilities discussed in the preceding section. The challenges addressed by the wind tunnel design includes optimization of the test facility productivity, aerodynamics, acoustics, pulsation mitigation, climate control, energy efficiency, and operational safety. The discussion of the wind tunnel key features is organized below according to these design challenge categories. It is often the case, however, that a given feature plays a role in multiple of these categories. For example, turning vanes are primarily an aerodynamics feature and are used in non-acoustic wind tunnels, but acoustically-treated turning vanes are very effective acoustic insertion loss elements. Turning vanes, therefore, will be discussed in both of these categories according to function.

Productivity Design Features

Facility productivity was an overarching criterion from the outset of the HALO wind tunnel design. Productivity factors into elements ranging from sequenced testing, test vehicle modifications and exchanges, deployment of measurement equipment, and reconfiguration of the test chamber for different test capabilities.

Testing is carried out using a supervisory control system which governs every aspect of the simulated test condition as well as the measurement systems and data recording functions. Test plans are pre-programmed into sequences which are then executed by the system, ensuring maximum test-time productivity and repeatability.

The time required to make modifications to a model within the test section is minimized due to the rapid acceleration and deceleration available from the main fan, which includes active braking. Modifications to vehicle underbody components are enabled by four lifts incorporated in the rocker panel restraints of the 5-belt MGP

module or by wheel lifts integrated into the turntable, which can be used with either 5-belt or single belt MGP modules.

Rapid exchanges of test vehicles are possible using two pathways between the vehicle preparation areas in the support building and the test section. A vehicle may be simultaneously removed from the test section through doors in the high-speed diffuser while a second vehicle is brought in through the vehicle access door in the downstream corner of the plenum. The new test vehicle may be rolled straight onto the turntable, which is rotated to align with the door.

Reconfiguration between aerodynamic and acoustic testing is partially automated. A flex floor is automatically raised to close the primary BLRS suction scoop to eliminate associated noise sources. The overhead array has automated deployment on rails, and stores in a room above the nozzle. The front array has automated deployment and stores within the test section towards the control room side. The overhead and front acoustic arrays automatically deploy or store in under two minutes. The side microphone arrays are manually deployed and are stored in rooms to either side of the nozzle. The side arrays are manually installed in under 10 minutes. A moving ground plane cover is used to achieve the lowest background noise levels, and its installation is manually performed in under 20 minutes.

Exchanging the 5-belt and single belt MGP modules requires approximately four hours. This process involves disconnecting the modules from supply lines for power, communications, and cooling as well as from the balance. The modules are lifted out of position by a semi-gantry crane, as seen in Figure 6, and transported into the wind tunnel infield for storage and maintenance.



Figure 6. Semi-gantry crane is used to transport MGP modules between the infield storage area and the turntable.

Changes between the large and small nozzle configurations are fully automated. To change to small nozzle, the operator makes a selection at the wind tunnel control console, and the system automatically flexes the side walls inwards, and the ceiling is flexed downwards to seal against the tops of the side walls at their inward-most position. The switch back to large nozzle is this same process in reverse and switching in either direction takes approximately two minutes.

Aerodynamic Design Features

The aerodynamic features of the HALO wind tunnel define the wind speed performance envelope, flow quality, and aerodynamic efficiency of the facility. These are primarily the main fan, the airline

circuit geometry, the turning vanes, and the features of the test section, which include boundary layer controls and the moving ground plane systems.

Main Fan

The main fan was supplied by TLT-Turbo and is shown in Figure 7. It has an 8.0 m diameter and is equipped with 12 carbon fiber fan blades and 15 stators/anti-swirl vanes. The fan is powered by a 5 MW motor that is housed within a 4.515 m diameter nacelle. Cooling air for the motor is pumped into the nacelle through one of the stators and is exhausted through a separate stator. Stators also house pass-throughs for electrical connections between the motor and the variable-frequency drive and wiring for temperature and vibration health monitoring of the bearings and motor windings.

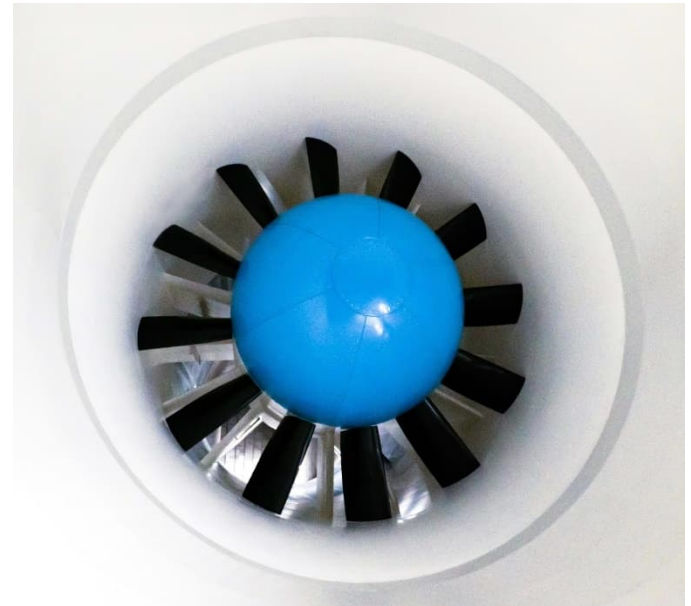


Figure 7. The main fan as viewed from upstream.

A foreign object debris (FOD) screen is attached to the trailing edges of the corner 2 turning vanes upstream of the fan, to protect the carbon fiber blades from damage. The fan inlet is a duct that transitions from the 9 m x 9 m square outlet of corner 2 to a 9 m circular cross section, followed by a contraction to an 8 m diameter to match the fan. The contracting fan inlet section improves flow uniformity, which enables the fan to achieve high efficiency, low noise, and lower cyclical structural loading. The additional contraction between circular sections just upstream of the fan thins the boundary layer through which the fan blades must sweep, and this further improves fan aerodynamics and acoustics.

Diffusers

The fan discharges through an annular diffuser, where the center body is formed by the nacelle tail cone. The annular diffuser connects to the backleg diffuser, which leads the flow to corner 3. These tandem diffusers work together to expand the flow by a factor of 3.35 from the fan annulus area of 34 m² to the corner 3 inlet area of 115 m². The significant diffusing section of the wind tunnel, the high-speed diffuser, is in the test leg. This diffuser expands by a factor of 1.57 from 43 m² at the outlet of the test section to 67 m² at the inlet to corner 1.

The function of the diffusers is to slow the flow down while recovering static pressure, and this creates an adverse pressure gradient that can encourage flow separation from the airline surfaces. Flow separation results in higher losses and therefore reduces circuit efficiency, but also is fundamentally an unsteady flow phenomenon and can adversely affect wind speed stability as sensed in the test section and also generate additional background noise. Therefore, careful design of the diffusers was performed using established guidelines and prior project experience.

Turning Vanes

There is a set of turning vanes in each of the four corners of the HALO wind tunnel. The primary function of any set of turning vanes is to guide the flow through the corner while promoting flow uniformity at the discharge side and with minimal pressure losses. However, the design of each set of turning vanes is different because each is optimized for a unique set of considerations.

There are a relatively small number (six) of corner 1 turning vanes due to acoustic self-noise considerations, which are discussed in the Acoustic Design Features section. There are eight turning vanes in corner 2, which is a number that balances the acoustic absorption properties of these vanes against the design goals of good discharge side flow uniformity with small wake structures for the sake of the main fan inlet aerodynamics. The corner 3 turning vanes are highly optimized for acoustics, but also turn the flow through less than 90 degrees. The heat exchanger placement on the diagonal of corner 3 produces a significant deflection of the air flow, so the turning vanes layout was carefully aligned with this effect, and this was one of the areas where computational fluid dynamics (CFD) was a critical design tool. More discussion of how CFD contributed to the HALO wind tunnel design is provided in the Design Development section.

The corner 4 turning vanes are optimized for aerodynamics as opposed to acoustics. Here, 22 double circular arc vanes with short chords are used to provide maximum uniformity at the inlet to the stilling chamber. The short chord length of the vanes minimizes the length scales of the turbulent eddies generated by their wakes and therefore speeds up the decay of this turbulence prior to entering the flow conditioning elements.

Stilling Chamber

The stilling chamber houses a honeycomb flow straightener and a single flow conditioning screen. The honeycomb flow straightener removes most of the vertical and lateral components of the flow, leaving flow aligned with the axis of the test section centerline. The flow conditioning screen improves flow uniformity and attenuates turbulence.

The 4.34 m space between the honeycomb and screen is much larger than typical for similar wind tunnels. This space provides room for the decay of turbulent eddies in the wakes of the honeycomb. A very low turbulence level impinging on the flow conditioning screen reduces the wind noise generated by the screen and also contributes to the low turbulence levels that were measured in the test section. The space between flow conditioning elements also provides ample room for inspections and maintenance.

Contraction and Flex Nozzle

The diffusion ratios discussed above enable the use of a relatively large contraction ratio compared to similar contemporary wind tunnels, at 7:1 for the large 25 m² nozzle and 10:1 for the small 18 m² nozzle. A large contraction ratio improves flow uniformity, angularity, and turbulence intensity. The lower flow speeds through the stilling chamber elements also reduces self-noise. The HALO contraction contour is a design that balances flow quality, minimization of boundary layer thickness in the nozzle, and noise generated from boundary layer interaction along the surface. The contraction forms a “picture frame” for the large nozzle, such that each of the sides, ceiling and floor surfaces displace by an equal amount towards centerline from the stilling chamber to the nozzle and have matching curvature profiles.

The main purpose of the flex nozzle is to reduce the fan power required for the high wind speeds typically only used for motorsports testing, and this is discussed in the Energy Savings section. The flex nozzle consists of specially-fabricated steel plates attached to a system of jacks that are mounted to the wind tunnel concrete structure. The large nozzle measures 3.86 m tall by 6.50 m wide, and the small nozzle is 3.30 m tall by 5.44 m wide.

The nozzle contains exit angle adjustability via steel plates designed to flex that were used for tuning of axial static pressure distribution (ASPD) and flow angularity during the aeroacoustic commissioning. The nozzle exit angle was fixed after commissioning.

Test Section

The test section is a large plenum which encompasses the ¾ open jet, the turntable with MGP, the collector, and the primary instrumentation discussed in the Measurement Systems section. The jet is 15.2 m long, which was set based on balancing the collector’s influence on the ASPD. If the jet length were shorter this would reduce fan power and low-frequency pressure fluctuation, but the static pressure rise upstream of the collector would interfere with accurate vehicle wake simulation. A longer jet would place the static pressure influence of the collector too far from the relevant test volume and would eliminate the ability to tune the ASPD via collector modifications during commissioning.

Collector

The aerodynamic roles of the collector are to capture the jet and shear layer flow and direct the flow into the high-speed diffuser and allow for tuning of the ASPD during aeroacoustic commissioning, while mitigating low-frequency pulsations and noise generation. The collector installed in the HALO wind tunnel is a new design, which is optimized for these functions.

The collector design incorporates swept leading edges with large radii, adjustable-angle side panels, and a fixed horizontal top panel with a trailing edge gap. There is a diffuser leading edge extension which places the trailing edge gap a short distance away from the downstream wall of the plenum. Tuning of the side panel angles and the trailing edge gap to control the upstream influence on static pressure and the generation of noise from impinging flow and the energetic flow through the trailing edge gap was performed both during design development and during aeroacoustic commissioning.

Discussion of the CFD and model-scale wind tunnel efforts that went into the collector design is provided in the Design Development section, and further discussion of the collector's roles in acoustics and low-frequency pulsation mitigation are discussed in the respective following sections.

Moving Ground Plane and Force Balance

The HALO wind tunnel has a turntable which incorporates modular moving ground plane (MGP) modules. This allows the wind tunnel to be configured with either a single belt MGP or a 5-belt MGP module. For either module, the functions provided by a MGP are to accurately replicate the relative motion between the ground surface and the vehicle when driving on roads. The MGP avoids the creation of a boundary layer on the ground surface and is also used to spin the vehicle wheels during testing.

The turntable allows for the vehicle and MGP to be yawed relative to the test section centerline. This enables simulation of cross-wind or side-skidding conditions where the vehicle nose is not pointed directly into the oncoming wind.

Single Belt Moving Ground Plane and Balance Connections

The single belt module provides the most accurate under-body wind simulation over the entire vehicle span and is critical for the study of flows around front spoilers and skirts typically associated with motorsports. The single belt is 3.2 m wide and the center-center spacing of the front and rear rollers is 9.5 m. The single belt is capable of operating up to 310 km/h.

The single belt configuration includes multiple components for force measurement. Vertical forces at the wheel contact patches are each measured by a wheel force measurement unit integrated into the air bearings under the belt. Longitudinal and lateral forces from the wheel contact patches acting on the belt are coupled to the 6-component balance. The vehicle restraints, as seen in Figure 2, include load cells to measure forces transmitted through the restraints. The forces and moments at all points of contact with the test vehicle are thus measured.

One challenge that is encountered when including a moving belt in force measurement is spurious forces due to the interaction of this belt with the surrounding air, including on the underside of the belt and the front and rear-facing surfaces of the belt as it wraps around the upstream and downstream rollers. Air is dragged along by the belt, and this results in friction and uneven pressures which sum up to force on the belt which is sensed by the balance.

Some of the spurious force can be characterized at different wind speeds and turntable angles without the presence of a vehicle. However, the spurious forces are sensitive to the blockage and wake effects when a vehicle is present. The HALO wind tunnel single-belt moving ground plane was designed to minimize the variability of spurious force due to the presence of a vehicle. This includes the use of wipers at specific locations to block entrained air flow and shield the belt from the pressure field generated by the test vehicle.

5-Belt Moving Ground Plane and Balance Connections

The 5-belt moving ground plane includes a 1.1 m wide and 9.5 m long center belt and four wheel drive units. The wheel drive units are small belts on which the vehicle tires sit and are used to spin the

wheels for aerodynamic simulation. The vehicle is held in place by the rocker panel restraints, which are posts that extend up from the balance and attach to the vehicle rocker panels just behind the front wheel wells and just in front of the rear wheel wells. The rocker panel restraints also allow precise setting of the vehicle ride height. The wheel drive units and rocker panel restraints are connected directly to the force balance within the turntable.

The spurious force concept that was discussed for the single belt moving ground plane applies also to the four wheel drive unit belts, but not to the center belt, since the latter is not connected to the balance. The spurious forces acting on the wheel drive units are much smaller due to their smaller size. The wheel drive units are 340 mm long between front and rear rollers and may be configured to be either 280 mm or 360 mm wide. The narrower width is preferred to minimize spurious force and the wider belts are used when necessary to accommodate very wide tire contact patches.

The 5-belt moving ground plane can be operated at speeds up to 270 km/h. The main advantages of the 5-belt moving ground plane over the single belt are more direct coupling between the vehicle and balance, ease of ride height adjustment, and reduced spurious forces.

Boundary Layer Removal Systems (BLRS)

The BLRS improve the aerodynamic simulation near the ground plane. The primary boundary layer system consists of a scoop in the nozzle upstream of the turntable which is responsible for extracting the boundary layer that forms along the floor of the contraction. The flow through the scoop is energized by a fan in the infield basement and is then ducted to a re-injection slot located in crossleg 1-2.

The secondary BLRS is located on the turntable just upstream of the moving ground plane. There is a suction slot which is responsible for extracting the boundary layer that has formed on the fixed portion of the floor downstream of the primary BLRS scoop. The secondary BLRS also has a blowing slot, which blows air tangentially over the upstream end of the moving ground plane. Tangential blowing energizes the flow directly above the floor and allows tuning of the flow profile directly above the MGP. The combination of suction and blowing slots located closely together also minimizes the BLRS impact on static pressure distribution and flow angle compared to a suction-only or blowing-only system.

The secondary BLRS suction and blowing slots span 3.4 m, and the blowing slot contains nine sections of variable-porosity loss elements that are independently adjustable. The secondary BLRS suction flow rate, blowing flow rate, and the blowing slot loss elements were each tuned during aeroacoustic commissioning to provide laterally uniform boundary layer profiles over the belt for any wind speed.

The tertiary BLRS is integrated into the 5-belt MGP module and removes the boundary layer that develops downstream of the secondary BLRS and upstream of the front wheel drive units. The tertiary BLRS also includes tangential blowing over the wheel drive units. The tertiary BLRS suction and blowing slot pairs are each 455 mm wide.

Acoustic Design Features

The acoustic design features of the HALO wind tunnel are responsible for achieving two design goals: very low background noise spectra levels with wind on and an anechoic test environment.

These are the two critical functions for a test facility to produce high signal-to-noise ratio when performing vehicle aeroacoustic testing.

Test Section Acoustic Test Environment

The test section walls and ceiling are clad with acoustically absorbent panels which were designed to attenuate noise in the 50 Hz to 20 kHz band. The cladding is integrated into all doors and access panels. The two large windows for the control room and observation room have acoustic covers that can be extended to prevent reflections off the glass surfaces. The control room windowpane on the test section side is set at an angle so that if the acoustic cover is not extended sound from the test vehicle will be reflected upwards and not straight back to the microphones. The test section volume was designed so that the microphone arrays could be placed at least ¼ of the longest wavelength of interest away from the nearest surface while also staying outside of the open jet shear layers.

The collector is clad with acoustic treatment to prevent noise reflections, and also has leading edge treatment with pile fabric to minimize noise generation from impinging flow. Discussion of the use of pile fabrics for noise reduction is provided by Nishimura et al. in [2]. Sections of the collector exposed to high-speed grazing flow are clad with diffusion-bonded paneling which developed to provide an acoustically-transparent surface which produces a minimum self-noise. Development of the diffusion bonded panel is discussed in [3].

The test section upstream and downstream walls includes large breathers that open to the outdoors. The breathers are each made as an “S-bend” acoustically-lined duct so intrusion from outdoor noise sources is minimized. The plenum acoustic treatment, collector, and breather silencer ducts were supplied by Faist Anlagenbau GmbH.

Fan Noise Mitigation

The most significant noise source during wind tunnel operation is the main fan. The fan selected for the HALO wind tunnel was specified and demonstrated to have minimum noise generation for the acoustic test design points. The acoustic design features of the main fan are beyond the scope of this paper. Noise from the main fan may reach the test section primarily through either the upstream path through corners 2 and 1 or through the downstream path through corners 3 and 4. The majority of the wind tunnel circuit is acoustically treated for the purpose of preventing transmission to the test section. 350 mm deep cladding covers the walls of all corners and both crosslegs, as well as the walls and ceiling of the high-speed diffuser and stilling chamber. The floor, walls, and ceiling of the contraction are lined with acoustic treatment.

Each set of turning vanes is acoustically treated to absorb sound on both inward and outward faces. The turning vanes of corners 1 and 3 feature trailing-edge extensions and the turning vanes of corner 2 feature leading and trailing edge extensions. These sets of turning vanes act very effectively as acoustic baffles with high perimeter to flow cross-section area for absorbing sound and prevent any direct line-of-sight between inlet and outlet.

The fan outlet annular diffuser includes acoustically lined external surfaces and tailcone. TAB Ingenieure GmbH supplied the wind tunnel circuit acoustic treatment, the turning vanes, and the fan outlet and tailcone.

Moving Ground-Plane Noise Mitigation

The moving ground plane system requires some gaps in the test section floor between moving and stationary components, and the belts of the 5-belt module have roughness to approximate road surfaces. These characteristics result in increased boundary layer noise generation compared to a completely smooth surface. Compressed air and vacuum must be supplied to the air bearings beneath the belt to prevent the possibility of lift at significant wind speeds, and these are additional noise sources both from the air flow through the bearings but also from the equipment.

Acoustic testing in the HALO wind tunnel may be performed in “quick acoustic mode” or in “quietest configuration”. For the former case, the moving ground plane systems remain operational but at reduced capacity to minimize noise. There are also passive noise controls; the compressed air and vacuum lines are insulated, and the underside of the turntable is acoustically lined to reduce noise intrusion into the test section. The compressors and vacuum system are located in the basement of the wind tunnel infield in a room which is isolated from the wind tunnel by thick concrete walls.

For the quietest configuration a smooth cover is installed over the moving ground plane. This cover is made up of 11 interlocking segments and is 4510 mm wide, 9950 mm long, and 8.4 mm thick. The cover may be installed in under 20 minutes. The MGP acoustic cover eliminates the extra boundary layer noise from roughness and gaps and allows for a test section without compressed air or vacuum systems applied to the MGP air bearings. Background noise levels measured in the test section with the MGP exposed and in quietest configuration are included in the Aeroacoustic Acceptance Testing section.

Flex Floor for PBLRS Scoop Closure

A significant noise source within the test section is the primary boundary layer removal system (PBLRS) scoop. The HALO wind tunnel includes a section of flexible floor upstream of the scoop, as seen in Figure 8. The upstream floor raises to cover the scoop and flexes at appropriate locations to maintain the contraction contour, leaving only a single seam between the floor and the lip of the scoop. These parts were precisely aligned during installation and a seal prevents air leakage or fluttering.

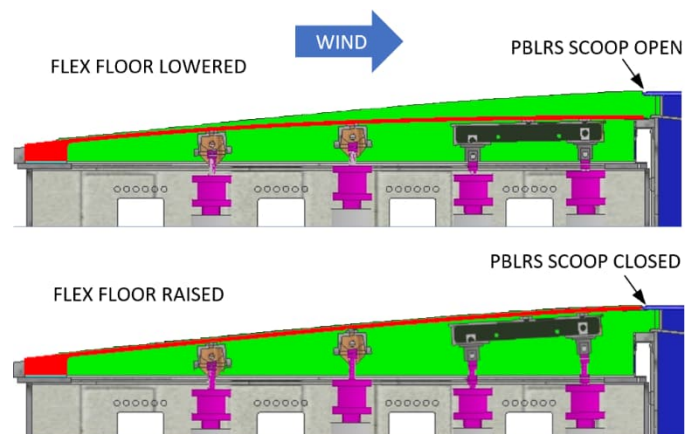


Figure 8. Flex floor and jacks upstream of the primary boundary layer removal system scoop.

Reduction of Other Noise Sources

The HALO wind tunnel includes many features to minimize test section noise intrusion from secondary noise sources.

- The flex nozzle incorporates extensive seals to prevent air leaks and associated noise.
- The test section floor, including the turntable, has stringent specifications for steps and gaps.
- The walls and ceiling of the high-speed diffuser and portions of corner 1 and the corner 1 turning vanes are covered in smooth fiberglass cloth to reduce self-noise generation.
- The corner 1 turning vane leading edges are covered in pile fabric to reduce flow impingement noise, and corner 1 has relatively few turning vanes and therefore less leading-edge surface area.
- The flow speed in corner 1 and associated wind noise is reduced due to the large diffusion ratio of the high-speed diffuser as compared to comparable aerodynamic wind tunnels.
- The only structural bracing “splitter plates” used in corner 1 are at the downstream end and not in line-of-sight to the test section.
- The FOD screen is attached to the trailing edge of the corner 2 turning vanes, so any noise generated will be attenuated by two sets of turning vanes before reaching the test section.
- The heat exchanger is on the diagonal of corner 3, which reduces flow speed through the heat exchanger and therefore noise generation. Heat exchanger noise is attenuated by two sets of turning vanes before reaching the test section, as well.
- The flow conditioning screen is placed sufficiently downstream according to the honeycomb-screen noise generation interaction, as described in [4].
- The acoustic treatment of the contraction has micro-perforated sheet cladding to reduce wind noise generation.
- The wind tunnel structure is concrete, and all doors into the wind tunnel have a sound transmission class (STC) of 55 or higher.
- The primary BLRS reinjection slot is positioned in crossleg 1-2 rather than within the test leg to avoid unsteady separated flow due to the backward-facing step inherent to this feature.

Low-Frequency Pulsation Mitigation Design Features

The driving function that causes low-frequency pulsation problems for open-jet and $\frac{3}{4}$ open-jet wind tunnels is the collector feedback mechanism [5,6,7]. The collector feedback mechanism results from vortices that detach from the nozzle to be convected downstream by the jet shear layer until coherently impacting the collector leading edge. The periodic vortices impinge on the leading edge surfaces and generate an unsteady pressure that propagates as infrasonic waves back to the nozzle and can synchronize with subsequent vortex detachments from the nozzle. The collector feedback mechanism tends to increase in strength with increasing jet length to hydraulic diameter ratio [8].

Collector feedback modes can couple with standing wave modes related to the airline circuit length and plenum width. When this happens it is possible to create intense low-frequency tones which

interfere with aerodynamic simulation and wind noise measurements. Strong pulsation tones correspond with increased average static pressure towards the downstream end of the test volume, and this results in erroneously low drag measurements due to horizontal buoyancy. The low-frequency pulsation effect varies with wind speed, so this problem can manifest as inconsistent drag coefficients over the range of test wind speeds.

Low-frequency pulsation is typically mitigated either by weakening the collector feedback mechanism or by disrupting the coupling of this mechanism with standing waves in the wind tunnel circuit.

Collector Feedback Mechanism Mitigation

The collector installed in the HALO wind tunnel has swept leading edges, as seen in Figure 9, and these cause any given shear layer vortex to impinge upon different portions of the leading edges at different times. This breaks up the coherence of the resulting pressure fluctuation, and significantly reduces the peak-to-peak pressure variation that is transmitted back to the nozzle.



Figure 9. The collector in the HALO wind tunnel test section features swept leading edges covered with pile fabric.

Standing Wave Mitigation

The HALO wind tunnel has two features which minimize standing waves effects. A series of five Helmholtz resonators were sized to address the 2nd through the 6th organ pipe modes of the airline circuit. The first mode was not addressed as this mode was observed to not be commonly problematic in existing wind tunnels and because the size of the resonator would be impractical. The resonator sized for the 2nd organ pipe mode has an internal volume of approximately 2000 m³. The two larger resonators are nested in the wind tunnel infield and are connected to crossleg 1-2. The three smaller resonators are connected to the downstream side of corner 2 and are located outboard of the airline circuit. Each resonator is connected to the airline through a neck with adjustable length to allow for fine tuning. The resonator sizes and locations relative to the airline were studied in the model scale test program, and this is discussed in the Design Development section. More discussion of the implementation of variable-length resonator necks is provided by Nagel et al. [9].

One of the innovations also tested in the model scale test program was the anti-resonant test section plenum design. This was achieved

by placing the side walls of the plenum at an angle to each other of approximately 6 degrees (combined). This was found to be sufficient to prevent any standing wave from forming between these large surfaces, which traditionally have been parallel. Standing waves related to the test section width have been measured for wind speeds above 220 km/h in other open jet wind tunnels with parallel plenum walls [10]. The success of this approach can be observed in the Campbell diagram presented in the Aeroacoustic Acceptance Testing and Results section (Figure 24). A plenum lateral mode standing wave would appear in this diagram as an energetic region in the 9-10 Hz range, based on the plenum width. However, no significant pulsations were noted in this frequency band regardless of microphone position in the test section or wind speed.

Temperature and Humidity Control Design Features

The wind tunnel climate control includes air temperature and humidity regulation. Air temperature control is provided via a heat exchanger located in corner 3. Cooling for the water/glycol loop is provided by six chillers with a combined capacity of 7.4 MW. A 2.5 MW electric heater is used for heating transitions and for temperature stabilization during large changes in air speed, such as rapid deceleration events.

Most of the energy required to change wind tunnel air temperature goes into changing the temperature of the wind tunnel structure, which is largely concrete. Most of the airline is clad with acoustic treatment, which provides some thermal insulation. Insulation is also included on the ceilings of the wind tunnel corners and crosslegs to further reduce the concrete's influence on air temperature.

Humidity control is achieved using continuous injection of dry air from the makeup air unit (MAU) and steam injection. The MAU provides dry air at a constant 20 °C temperature to the balance room, which helps keep the balance temperature constant regardless of test section conditions. The balance room has openings to the test section that are hidden behind the side walls of the collector. These openings permit the dry air to be introduced while isolating any noise transmission from the test volume.

Energy Efficiency

The main energy consumers for wind tunnel operation are the main fan and cooling systems, followed by the MGP, BLRS, MAU, and auxiliary systems. It is possible to select cooling systems with lower power requirements than the active chillers used for the wind tunnel. However, these do not provide the level of air temperature control required for the HALO wind tunnel regardless of ambient weather conditions. The dominant heat load on the cooling system is the main fan power, so reducing main fan power requirements for a given test condition is the most effective means of saving power.

Fan power is directly proportional to the volume flow rate and the pressure losses through the wind tunnel circuit. The first of these factors is addressed by the use of the two-position flex nozzle, and this is the single largest contribution to energy efficiency of the HALO wind tunnel design. The flex nozzle is set to the 18 m² outlet area for the highest wind speeds, and this reduces volume flow rate throughout the circuit and so reduces pressure losses. However, this is partially counteracted by an increased jet length to nozzle hydraulic diameter ratio and an increased vehicle blockage ratio, and therefore increased pressure losses within the test section. The flex nozzle is responsible for an approximate 25% reduction in fan power to

achieve maximum wind speed, relative to having a fixed 25 m² nozzle exit area.

The high contraction ratio used in the HALO wind tunnel provides an energy savings benefit. The larger cross-sections throughout the closed-return circuit result in reduced flow speeds, which minimizes pressure losses through elements such as the heat exchanger, turning vanes, and flow conditioning elements, and therefore fan power. The power savings relative to comparable wind tunnel design with a 5.5:1 contraction ratio is approximately 13%. The high contraction ratio also benefits flow quality and minimizes noise generation from flow over the flow conditioning elements.

The final significant energy savings design feature is the location of the heat exchanger in the diagonal of corner 3, rather than in a more traditional location in the crossleg between corners 3 and 4. The increased heat exchanger area and corresponding reduction in air flow speed through it results in approximately 5% fan power savings. The heat exchanger location upstream of the corner 3 also provides the benefit of further isolating noises generated from flow through the heat exchanger from the test section.

The HALO wind tunnel main fan power was measured to be approximately 4.0 MW at 310 km/h with a vehicle C_DA of 0.72 m² with the small nozzle, and 3.0 MW at 250 km/h with a vehicle C_DA of 1.8 m² with the large nozzle.

Design Development

The HALO wind tunnel design leverages prior project experience wherever possible. However, innovations were necessary to produce a facility that would meet challenging performance requirements. As typical, the design phase included analysis, simulation, and testing. Some of the more notable activities performed during engineering design are discussed here.

Computational Fluid Dynamics

Computational fluid dynamics (CFD) analysis was performed extensively during the design phase. Steady-state Reynolds averaged Navier-Stokes (RANS) type CFD was used for evaluating diffuser and turning vane flow, as well as for examining flow uniformity at the fan inlet and in the nozzle outlet. RANS CFD analysis was used to optimize the BLRS geometry and to determine appropriate flow rates for the fans and flow meters.

Development of the new collector design was an area where CFD analysis provided a significant contribution. This was done prior to sub-scale wind tunnel testing with the new collector geometry.

Collector Design Plan

A number of recent or concurrent projects with the HALO wind tunnel had very low overall sound pressure level (OASPL) requirements. Aggressive OASPL performance targets meant that the collector became a focus as a primary influence on noise in addition to axial static pressure distribution (ASPD) and low-frequency pressure fluctuations. Scale model and advanced CFD methods were used to develop and evaluate options for an innovative collector design to provide exceptional performance.

Previous aerodynamic wind tunnels (such as BMW AVZ [10]) demonstrated very flat ASPD while employing a collector configuration using an inverted-airfoil i.e., airfoil with suction side facing toward airline centerline. The use of an airfoil collector provided a reliable control of flow quality and ASPD throughout the test volume. However, an innovative collector design was undertaken for the HALO wind tunnel to achieve ASPD, C_{pRMS} , and acoustic performance. A hybrid design was developed which incorporated a swept panel-style collector followed by a diffuser leading edge extension (DLEX) transition to the high speed diffuser. This design allows for adjustable in flap angle and variable recirculation flow via adjustable gap size between the collector and DLEX.

A Detached Eddy Simulation (DES) CFD campaign was undertaken to develop and evaluate the collector design. The CFD focused on velocity trends and comparisons of fluctuating velocities, collector loads and plenum pressures. It was understood early on that fluctuating and mean pressures on the collector leading edges correlate strongly with noise generation.

DES Simulation of Collector

The DES CFD was performed using Siemens Star-CCM+ software and application of the Improved Delayed DES variant solver model. This model better resolves the time-varying nature of vortex shedding flow emanating from the test section nozzle and being convected downstream in the shear layers of the jet, in comparison with steady-state RANS techniques. An isometric view of the 3D CFD domain can be viewed in Figure 10.

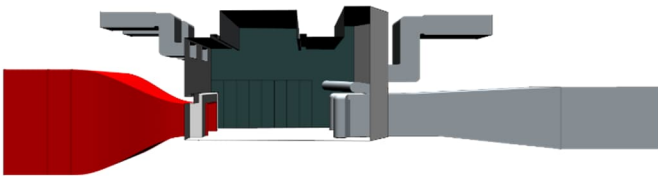


Figure 10. Three-dimensional CFD domain extents.

The inlet of the domain starts in the stilling chamber upstream of the honeycomb and screen. The domain carries through the test section and high speed diffuser before being truncated at a planar exit pressure boundary located at what would be corner 1 of the full wind tunnel airline. Upstream and downstream breather ducts were also included in the model to capture any secondary flow unsteadiness in the plenum due to air exchange with the outdoors.

The improved levels of time-accurate solution and solution resolution comes at the cost of significantly increased grid and computational costs. A view of the mesh and grid resolution for the jet and collector regions can be seen in Figure 11.

Prism layer mesh resolution at the walls of the contraction, test section floor, and collector were resolved to satisfy $Y^+ \leq 1$. The resolution of vortex structures in the free shear layers ultimately necessitated a mesh size on the order of 50 mm for cells within the test section and 10 mm at the nozzle exit plane (NEP). This led to total volume cell counts on the order of 130 million cells.

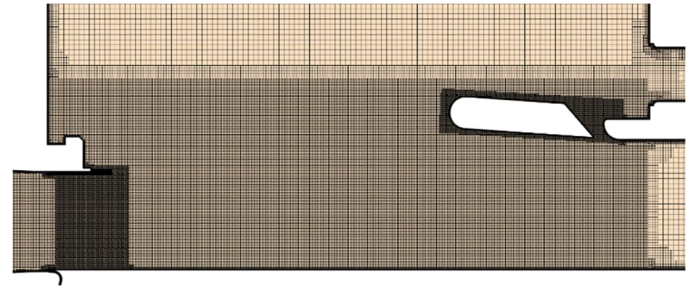


Figure 11. Global mesh resolution within the test section.

CFD Results

To accurately capture pressure wave fluctuations at or below 250 Hz, a second-order temporal discretization was employed with a time step of $1e-4$ s, which maintained local Courant numbers at or below 5. For this study the SST $k-\omega$ DES turbulence model was chosen which modifies the dissipation term in the transport equation for the turbulent kinetic energy. The convective Courant numbers associated with flow surrounding the collector can be seen in Figure 12. The secondary flow through the collector flap gaps is seen to be below a local Courant number of 5.

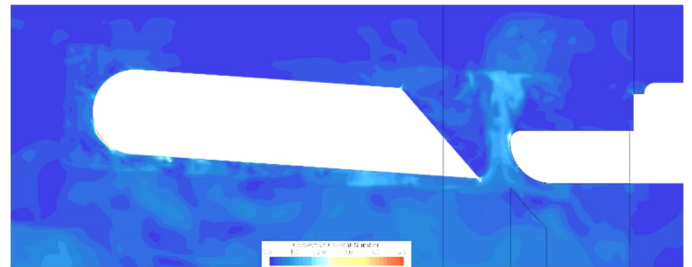


Figure 12. Local Courant number.

For the CFD simulations, each candidate collector configuration was analyzed at 250 km/h to match the maximum airspeed for large nozzle configuration. The instantaneous velocity magnitudes of flow in the test section are plotted in Figure 13. High speed airflow propagating from the nozzle is accelerated slightly due to shear layer expansion before being collected almost entirely by the collector and DLEX. Some secondary vortical flow is intermittently passed over the leading edges of the collector before being re-entrained by the primary core flow. A moderate stream of flow is allowed through the ceiling collector's rear gap, driven by recovering pressure gradients in the DLEX and high-speed diffuser.

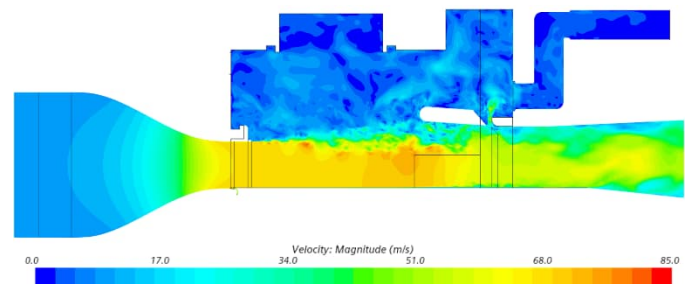


Figure 13. Test section velocity magnitudes on centerline.

The level to which the collectors capture high speed jet flow is further elucidated by the iso-surface depictions of flow at or below

20 m/s plotted in Figure 14. The shear layer expansion causes flow at or above 30% of test section speed to mostly pass directly from nozzle to collector. The relatively large plenum height and angled side walls further aid in flow speed diffusion to mitigate noise generated by flow gusting behaviors.

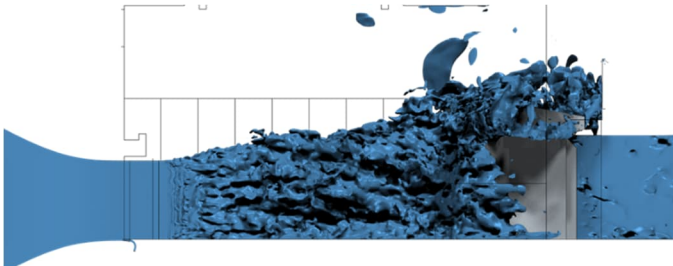


Figure 14. Elevation view of 20 m/s iso-surface flow.

Velocity Trends

Variations to the collector design were tested such as flap angles and trailing edge gap width. High or fluctuating flow speeds impinging on a plenum wall or at the locations where microphones are to be located during vehicle testing can cause undesirable noise. The out of flow (OOF) measurement location and plenum sidewall location sensitivity to side collector gap closure is plotted in Figure 15. The OOF measurement point is the standard acoustical location 6 m to the side of vehicle center.

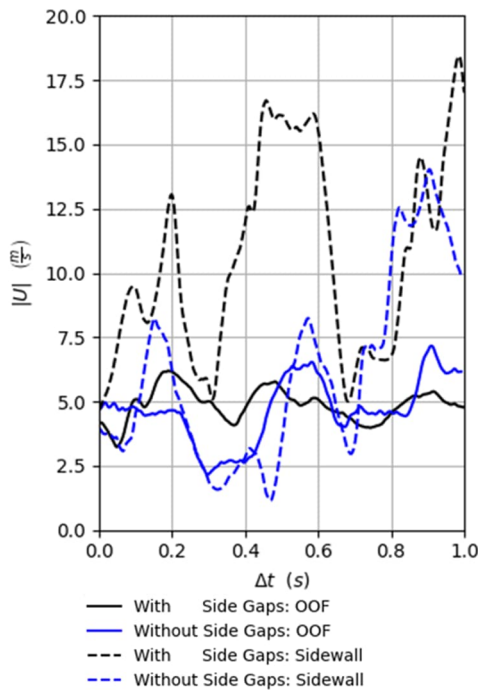


Figure 15. Velocity magnitude variation over simulation time at two locations in the plenum.

The predicted flow speeds at this location are not significantly changed by the breather gap modification. However, the predicted airspeeds grazing the plenum walls adjacent to the collector inlet plane indicate a roughly 40% reduction in average airspeeds and 24% reduction in maximum gusting flow for the case with a side collector gap closure. This insight from the CFD results was important for

understanding some of the noise sources related to the flow fields generated by the collector, and how the collector design should be optimized for the acoustic test environment.

Collector Loads

The CFD results were also used to define steady and unsteady loads on the collector components as shown in Figure 16. Average and standard deviation values of simulated lateral loads were calculated. The standard deviations were approximately 30% of the average values.

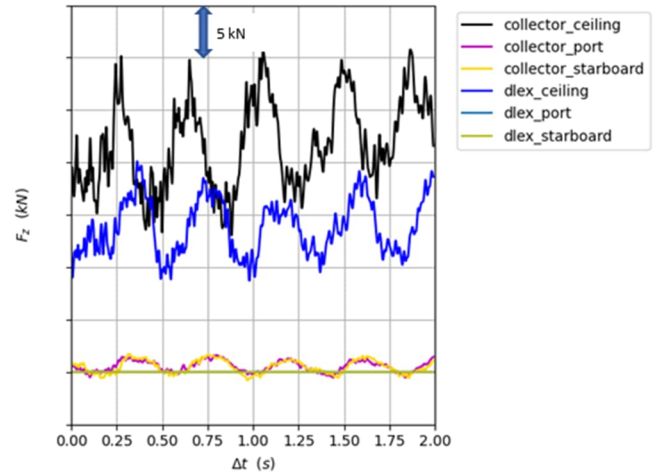


Figure 16. Time-varying vertical forces acting on the collector and diffuser leading edge extension.

Vertical loads on the diffuser leading edge extension (DLEX) and collector exhibit highly unstable behavior. The oscillating loads caused a standard deviation of $\pm 30\%$. The structure for the DLEX and collector must withstand the peak loads and must not have structural harmonics which may resonate with frequencies encountered in the unsteady aerodynamic loading. The calculated aerodynamic loads on the collector were validated during wind tunnel commissioning.

Model-Scale Testing

Model-scale testing was a crucial part of developing the design of the HALO wind tunnel. For the design of HALO it was desirable to study low-frequency pulsation to reduce the effect that it has on testing in an open-jet wind tunnel. Published work from past open jet wind tunnels shows that the cause of resonance is the response of the circuit duct to the collector feedback modes generated by the shedding shear layer [6]. It was therefore necessary for the scale model wind tunnel to be a complete closed-loop circuit. The scale model wind tunnel, seen in Figure 17, represents a 1:8 scaling of the HALO wind tunnel design, including most critically the circuit length, jet length, and nozzle geometry. These items were the first-order drivers of the C_{pRMS} and ASPD characteristics of an open-jet wind tunnel. Other components that have geometries exactly scaled include the collector, diffuser inlet, the plenum walls, and the ceiling. Acoustic treatment was added throughout the wind tunnel circuit following the initial infrasonic noise and ASPD study. This prepared the wind tunnel for evaluating the acoustic performance of components in the test section that affect background noise levels.



Figure 17. The 1:8 scale closed-return model wind tunnel during development testing.

Mitigation of Organ Pipe Resonance

Helmholtz resonators are a standard design tool that has been incorporated into several wind tunnel designs in the past 20 years [11]. It was determined that the focus would be placed on organ pipe modes 2 through 6 based on analysis of prior wind tunnel commissioning results, and this covers frequencies from 10 Hz to 40 Hz at the 1:8 scale. New for this project was a large resonator to cover the 2nd mode after recent results showed that this mode adds a significant amount of energy to the infrasonic pulsations, or Cprms.

While geometric sizing of resonators for different frequencies has been explored in previous work, one open issue was reliable placement of resonators at circuit locations which provide satisfactory damping. This occurs due to the interaction of pressure waves as they propagate in opposite directions around the circuit. Resonators placed at nodes will have minimal effect, and ideally a resonator tuned to a given frequency will be placed at an anti-node of a standing wave for that frequency. Several penetrations were made in the circuit duct from corner 1 to the downstream side of corner 2 to determine the optimal location of resonators. These penetrations allowed for the installation of resonators for modes 3 through 6 at any of the positions. The resonator for mode 2 was so large that it was restricted to a single location attached to the cross leg between corner 1 and 2. However, the wavelength of mode 2 is so large that this is the most generous mode with respect to flexibility of resonator placement.

The penetrations were blocked off and a speed sweep was performed to determine a baseline performance and define speeds where each mode was excited. Infrasonic microphones were then stepped through each of the penetration locations in an attempt to find anti-nodal points where resonators may be most effective. Many iterations of resonator geometry and location were investigated using speed sweeps to evaluate and compare configurations. It was determined that resonators tuned for the higher frequencies were ineffective in the crossleg, so resonators for modes 4, 5 and 6 were all placed downstream of corner 2. The resonators for mode 2 and 3 proved to be effective when located at the center of the crossleg. The results of the resonator study did not eliminate the infrasonic noise in the test section but did provide a measurable reduction and fed critical information about the optimal sizing and placement of resonators for the full-scale wind tunnel design.

Mitigation of Resonance in the Plenum

In addition to the resonance excited in the form of standing waves in the circuit ducting, the shear layer flow can also excite resonance in the test section. For a plenum with parallel side walls these standing

waves can reflect between the walls and typically arise at the higher operating speeds. This is visible in Figure 18 at 240 km/h and above at approximately 65 Hz, which corresponds to a half wavelength between the side walls. There are several other potential modes that can set up in the plenum excited by the shear layers of the jet.

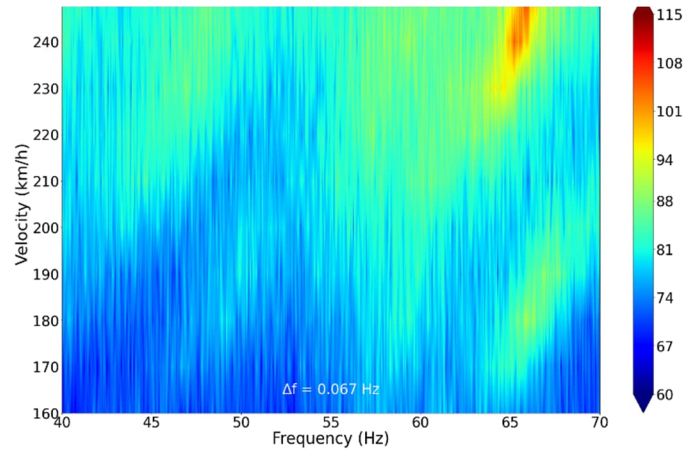


Figure 18. Campbell plot of model-scale plenum resonance with parallel side walls.

The proposed solution for the HALO wind tunnel was an anti-resonance plenum which incorporates walls with an expanding plenum width in the upstream to downstream direction, which can be seen in Figure 1. A proof of concept of this design was constructed in the plenum of the model scale tunnel. The test proved successful, showing a significant reduction in the plenum resonance, as evidenced by the significant reduction in activity near 65 Hz seen in Figure 19 as compared to Figure 18.

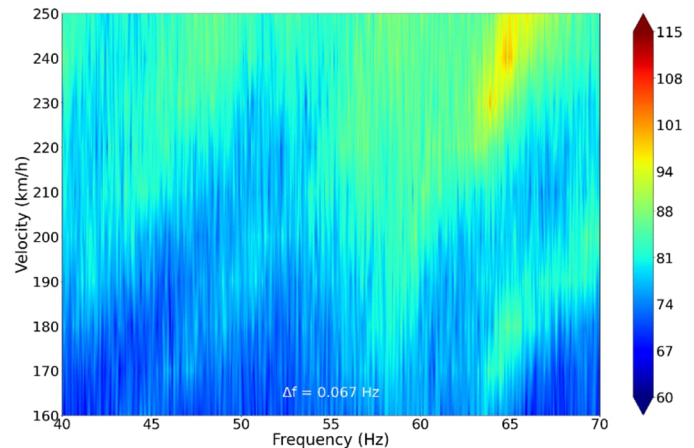


Figure 19. Campbell plot of model-scale plenum resonance with angled side walls.

Collector Design Development

Model-scale testing was used to continue the development of the collector design as a continuation of the design analysis started with CFD. Multiple collector configuration variations were tested to evaluate their effects on low-frequency pressure fluctuation, ASPD, and background noise levels. An interim configuration, prior to finalizing the side panel shape, is shown in Figure 20.



Figure 20. A model of the collector undergoing acoustic testing in the 1:8 scale model wind tunnel.

The design elements that were evaluated during model-scale testing for the collector and DLEX include: positioning, panel shapes and angles, leading edge radii, surface materials, and the gap sizing, shapes, and locations. The appropriate range of geometry adjustability was determined for the purpose of the full-scale aeroacoustic commissioning. The test program resulted in a collector and DLEX design with a significantly reduced background noise contribution, as seen in Figure 21.

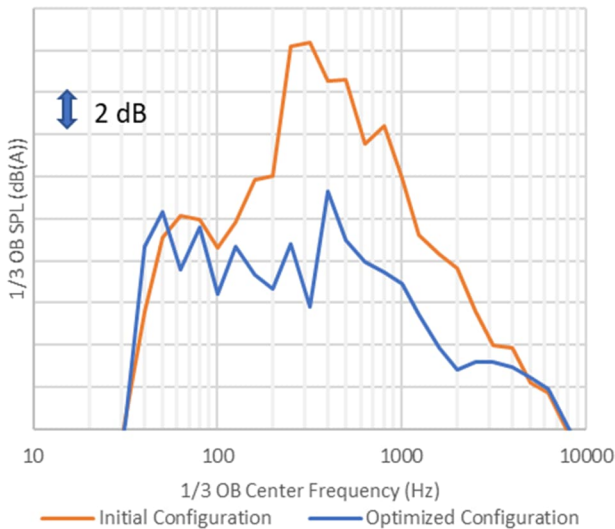


Figure 21. Reduction in background noise levels in the model scale wind tunnel resulting from test program design development.

Aeroacoustic Acceptance Testing

This section describes the critical results from the aerodynamic acceptance tests which characterize the aerodynamic simulation capabilities of the HALO wind tunnel. Aerodynamic calibration, commissioning, and acceptance test work was completed in February 2022.

The HALO wind tunnel coordinate system is in accordance with the SAE Surface Vehicle Recommended Practice [12] and originates on the centerline of the test section floor at the vehicle center, defined as the vehicle wheelbase and track intersection. This point is 5000 mm downstream of the nozzle exit plane and 500 mm upstream of the turntable center. The X-axis points downstream, the Y-axis points to the right as one looks upstream, and the Z-axis points vertically upwards. This arrangement is shown in Figure 22.

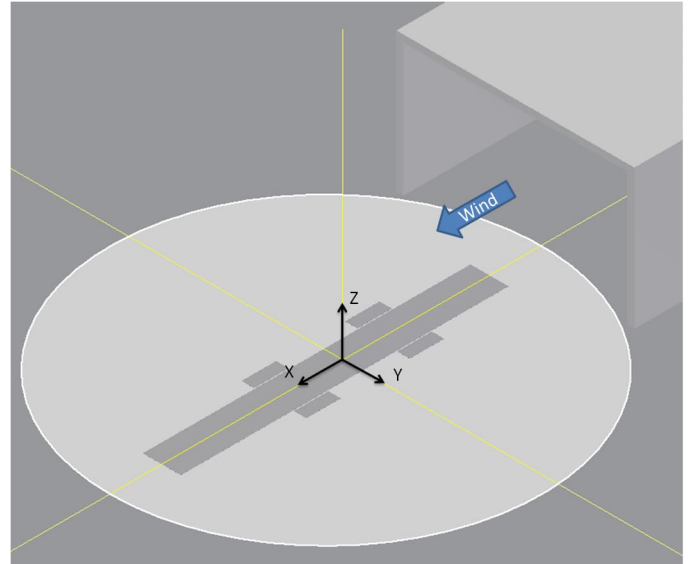


Figure 22. HALO wind tunnel coordinate system

The wind tunnel acceptance test results are presented in this paper under three categories: acoustics, aerodynamics, and climatic. Tables 3, 4, and 5 provide summaries of the test results for these categories, respectively.

Table 3. Summary of acoustic and infrasonic acceptance test results. Acoustic measurements were performed with the large nozzle.

Test	Result
Hemi-anechoic test section, ISO 3745:2017	Certified 50 Hz to 20 kHz
Background noise @ 100 km/h	OASPL = 47.8 dB(A)
Background noise @ 140 km/h	OASPL = 56.6 dB(A)
Background noise @ 160 km/h	OASPL = 60.5 dB(A)
Large nozzle $C_{p_{RMS}}$, 80 km/h to 250 km/h	$C_{p_{RMS}} \leq 0.44\%$
Small nozzle $C_{p_{RMS}}$, 140 km/h to 310 km/h	$C_{p_{RMS}} \leq 0.37\%$

Table 4. Summary of aerodynamic acceptance test results with the large nozzle.

Large Nozzle	
Test	Result
Vmax with $C_{DA} = 1.8 \text{ m}^2$	250 km/h
Vmax with $C_{DA} = 4.8 \text{ m}^2$	140 km/h
Wind speed stability at 250 km/h, $1\sigma(U)$	0.11 m/s
Acceleration time, 10 km/h to 250 km/h	29 s
Deceleration time, 250 km/h to 10 km/h	45 s
ASPD: range with $ C_p \leq 0.002$	$-3.5 \text{ m} \leq X \leq 4.5 \text{ m}$
Dynamic pressure uniformity: $1\sigma(C_q)$	
at 80 km/h	0.24%
at 120 km/h	0.22%
at 180 km/h	0.23%
at 250 km/h	0.17%
Flow angularity: mean($\bar{\alpha}, \bar{\beta}$), $1\sigma(\bar{\alpha}, \bar{\beta})$	
at 80 km/h	0.066°, 0.130°
at 120 km/h	0.058°, 0.142°
at 180 km/h	0.074°, 0.124°
at 250 km/h	0.059°, 0.106°
Turbulence intensity: max(u'/U), mean(u'/U)	$10 \text{ Hz} \leq f \leq 5 \text{ kHz}$
at 80 km/h	0.13%, 0.04%
at 120 km/h	0.11%, 0.04%
at 180 km/h	0.14%, 0.04%
at 250 km/h	0.17%, 0.06%
Boundary layer shape: u/U from 2 mm to 100 mm On centerline of 5-belt center belt	
at 80 km/h	1.001 – 1.012
at 120 km/h	0.999 – 1.006
at 180 km/h	1.000 – 1.008
at 250 km/h	1.001 – 1.007

Table 5. Summary of aerodynamic acceptance test results with the small nozzle.

Small Nozzle	
Test	Result
Vmax with $C_{DA} = 1.0 \text{ m}^2$	310 km/h
Wind speed stability at 310 km/h, $1\sigma(U)$	0.06 m/s
Acceleration time, 10 km/h to 310 km/h	40 s
Deceleration time, 310 km/h to 10 km/h	57 s
ASPD: range with $ C_p \leq 0.004$	$-2.5 \text{ m} \leq X \leq 4.5 \text{ m}$
Dynamic pressure uniformity: $1\sigma(C_q)$	
at 250 km/h	0.15%
at 270 km/h	0.15%
at 310 km/h	0.16%

Small Nozzle	
Test	Result
Flow angularity: mean($\bar{\alpha}, \bar{\beta}$), $1\sigma(\bar{\alpha}, \bar{\beta})$	
at 250 km/h	0.124°, 0.147°
at 270 km/h	0.124°, 0.148°
at 310 km/h	0.127°, 0.158°
Turbulence intensity: max(u'/U), mean(u'/U)	$10 \text{ Hz} \leq f \leq 5 \text{ kHz}$
at 250 km/h	0.07%, 0.04%
at 270 km/h	0.07%, 0.04%
at 310 km/h	0.07%, 0.04%
Boundary layer shape: u/U from 2 mm to 100 mm -1200 mm $\leq Y \leq$ 1200 mm with single belt	
at 250 km/h	0.994 – 1.011
at 270 km/h	0.996 – 1.014
at 310 km/h	0.991 – 1.004

Table 6. Summary of climatic acceptance test results. These tests were with the large nozzle.

Test	Result
Temperature uniformity: $1\sigma(T)$	
at 10 °C and 120 km/h	0.202 °C
at 20 °C and 140 km/h	0.096 °C
at 25 °C and 200 km/h	0.055 °C
Dew point stability: $1\sigma(T_{DP}(t))$	
at 10 °C and 120 km/h to 160 km/h	0.20 °C
at 20 °C and 120 km/h to 160 km/h	0.57 °C
Temperature transition times	
10 °C to 20 °C at 160 km/h	14.5 min
20 °C to 10 °C at 120 km/h	30 min
20 °C to 50 °C at 160 km/h	1 hr. 40 min
50 °C to 20 °C at 120 km/h	30 min

Hemi-Anechoic Free-Field Test Environment

The Hemi-Anechoic qualification was conducted by broadcasting a broadband random noise signal from an omni-directional loudspeaker placed on the floor in the center of the turn table.. The HALO wind tunnel test section was qualified as a hemi-anechoic free-field environment according to the standards of ISO 3745:2017 between 50 Hz and 20 kHz, within a 7 m radius of the turntable center.

Background Noise

The background noise level measurements were made for large and small nozzles with the 5-belt module in place with an empty test section. The test utilized a free-field microphone mounted on a tripod positioned at (X, Y, Z) = (0, -6, 1) m relative to the vehicle center, as seen in Figure 23.

The “quietest condition” tests were created by installing an acoustic cover over the moving ground plane (MGP); the boundary layer

removal systems were off, the secondary BRLS suction slot was covered, and the flex floor was raised. Figure 24 compares 1/3rd octave band spectra for the large nozzle with the quietest condition vs. MGP exposed condition at 100 km/h, 140 km/h, and 160 km/h. The MGP exposed condition entails all of the features of quietest condition except the MGP cover is not installed. The increase in noise that is measured with the MGP exposed can be attributed to the surface roughness of the belts, gaps between fixed and moving ground plane elements, and the operation of the air and vacuum bearings beneath the center belt to ensure it does not lift under wind.



Figure 23. Microphone mounted on stand and positioned at (X, Y, Z) = (0, -6, 1) m relative to vehicle center. The MGP acoustic cover was installed, and the turntable was yawed when the photo was taken.

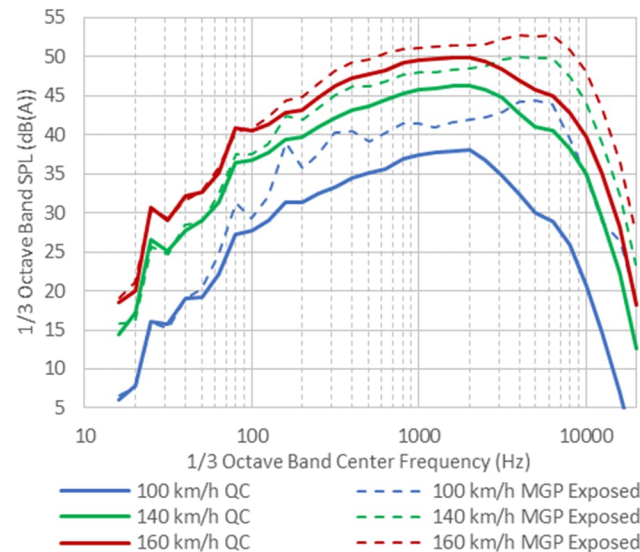


Figure 24. Background noise levels for the large nozzle with quietest condition (QC) and with MGP exposed.

Figure 25 shows the OASPL for the HALO wind tunnel in quietest condition versus wind speed. This chart includes published data from contemporary aeroacoustic wind tunnels in Europe, North America, and Asia for comparison [13,14,15,16,17,18,19,20].

The HALO wind tunnel background noise levels compare very well with the best automotive aeroacoustic wind tunnels. Extensive application of acoustic treatment throughout the wind tunnel, strict attention to surface smoothness within the test section, and optimization of the collector geometry using computational fluid dynamics and model-scale testing were necessary to keeping noise levels to these minimum levels.

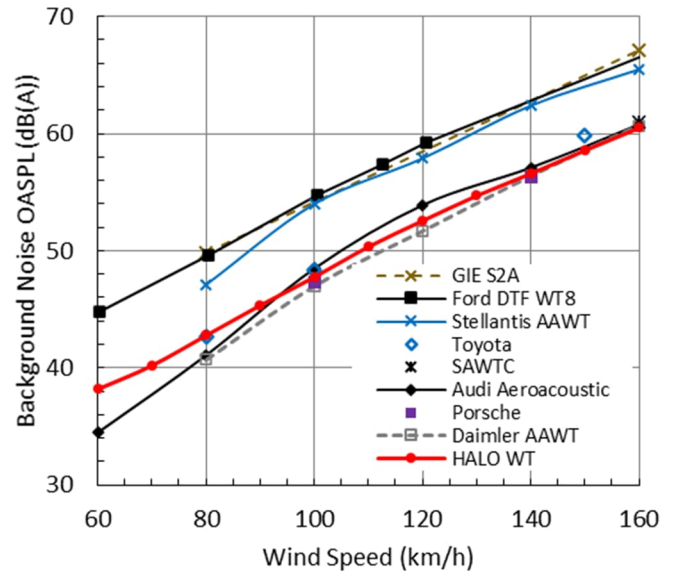


Figure 25. Background noise OASPL versus wind speed for the HALO wind tunnel and other modern aeroacoustic wind tunnels.

Plenum Pressure Fluctuations, $C_{p_{RMS}}$

The infrasonic RMS pressure coefficient, ($C_{p_{RMS}}$) is defined as the root-mean-square microphone pressure divided by the free stream dynamic pressure. $C_{p_{RMS}}$ values for the HALO wind tunnel are presented for out-of-flow and in-flow measurement locations in Figures 26 and 27, respectively. The out-of-flow measurement location was 6 m to the side of the vehicle center, towards the control room, and 1 m above the floor. The in-flow measurement location was directly above the vehicle center location, 1 m above the floor. Published values for other wind aerodynamic and aeroacoustic wind tunnels are included for comparison, with out-of-flow measurement results [9, 10, 15, 19] and in-flow measurement results [9, 10, 16, 21].

The bandpass used for calculation of $C_{p_{RMS}}$ for the HALO wind tunnel was 0.5 Hz to 20 Hz. The lower bound of this band was chosen as it is low enough to capture the first organ-pipe mode of the circuit but high enough to filter out very low-frequency atmospheric pressure fluctuations. Consideration must be given to bandpass when making comparisons to other published values.

A Campbell plot for the pulsation measurements with the large nozzle is shown in Figure 28. There is a distinct lack of any tone associated with a plenum mode, which would be expected in the 9 Hz to 11 Hz range.

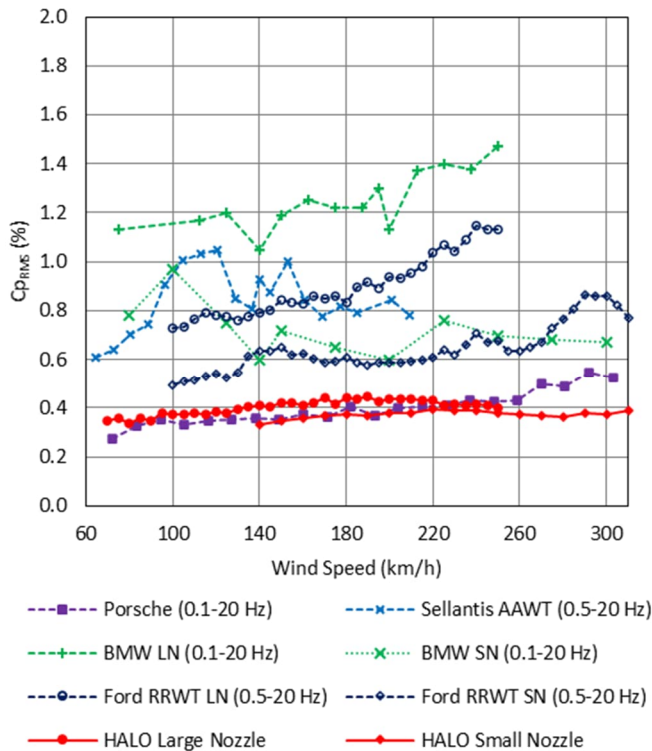


Figure 26. Out-of-flow C_{pRMS} versus wind speed, 6 m to the side of vehicle center.

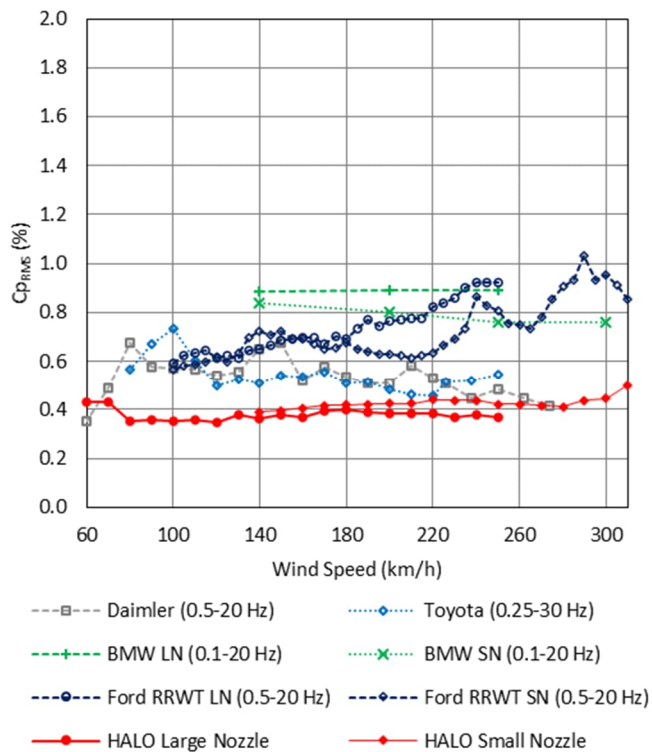


Figure 27. In-flow C_{pRMS} versus wind speed, at vehicle center.

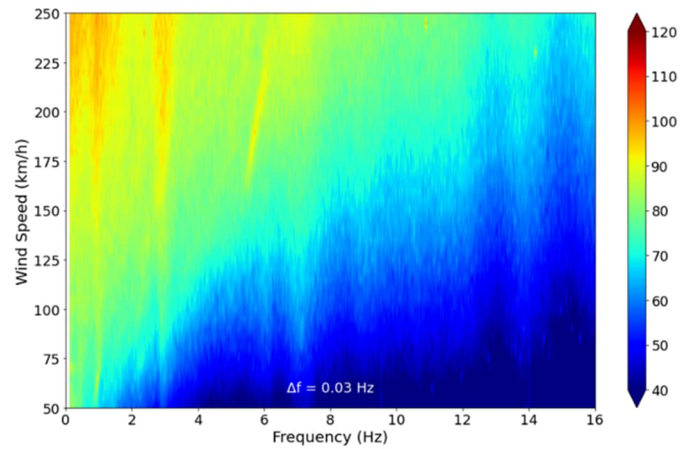


Figure 28. Campbell plot of low-frequency pulsation (C_{pRMS}) for the large nozzle configuration.

The low-frequency pulsation characteristics of the HALO wind tunnel compare favorably to similar modern wind tunnels. The HALO wind tunnel features: resonators which address organ pipe modes 2 through 6, swept collector, and anti-resonant plenum work together to provide a test environment in which pulsations remain consistently low without “tones” at any speed.

Consistent and low pressure fluctuation contribute to consistent vehicle drag measurement. Erroneously low drag coefficient measurements occur at wind speeds with problematic pulsations. These “notches” in the drag coefficient versus wind speed trend may be deeper than 0.01, as reported by Wickern et al. [18]. The drag coefficient of a passenger vehicle in the HALO wind tunnel with the large nozzle and 5-belt moving ground plane is presented in Figure 29. The trend shows a drag coefficient that varies smoothly with wind speed.

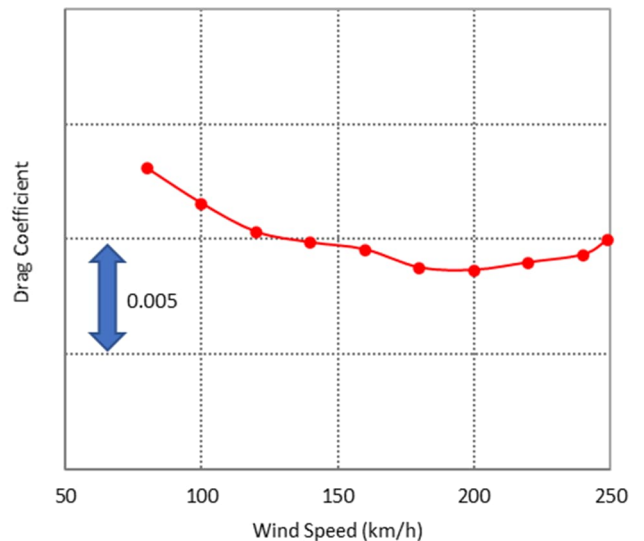


Figure 29. Passenger vehicle drag coefficient trend with wind speed.

Low C_{pRMS} also helps to avoid set of sympathetic vibration in windows, doors, and access panels, which could rattle and degrade the acoustic test environment.

Axial Static Pressure Distribution

The acceptance measurements for the axial static pressure distribution (ASPD) were performed along the centerline ($Y = 0$) of the wind tunnel at the height of $Z = 750$ mm above the ground. A pitot-static probe was used for the ASPD measurement and mounted on a carbon fiber boom, which was attached to the flow survey traverse. The measured data for the large and small nozzles at different speeds are shown in Figures 30 and 31, respectively.

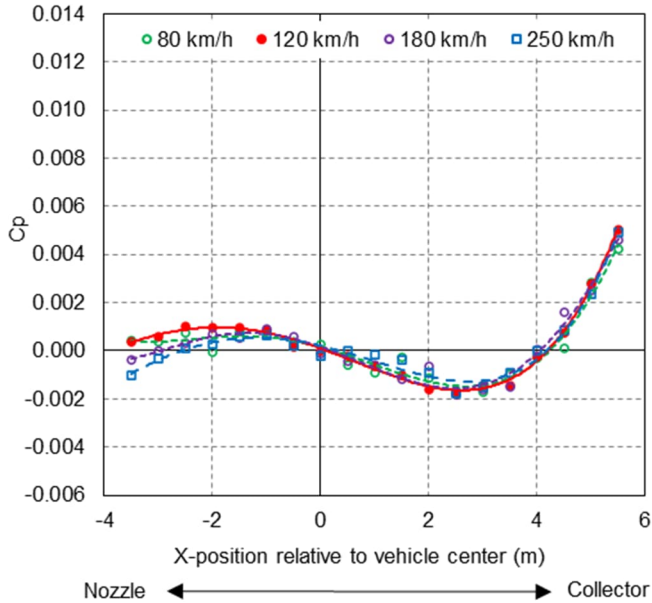


Figure 30. Axial static pressure distribution with the large nozzle

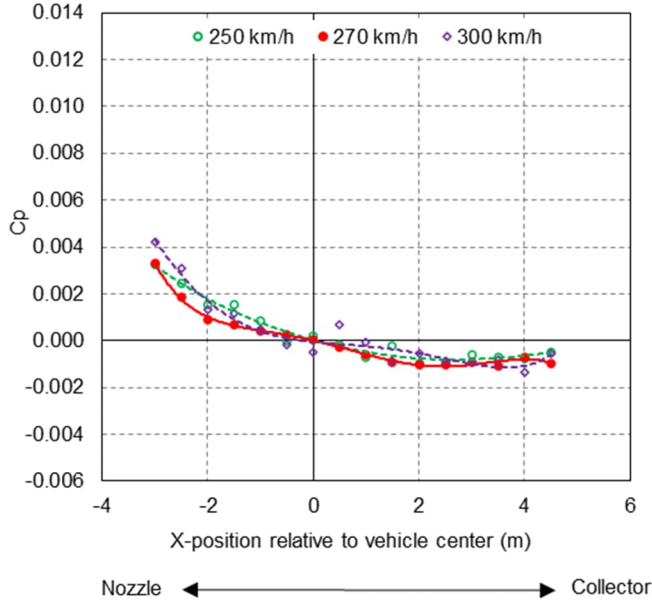


Figure 31. Axial static pressure distribution with the small nozzle

The tuning of the ASPD in the HALO wind tunnel consisted of adjustments to the nozzle exit and collector. The ASPD was optimized for the large nozzle, since the ultimate precision of drag coefficient measurements are more critical for passenger vehicle development than for motorsports. This is most evident upstream of the vehicle center. The pressure rise upstream of the collector is

prominent for the large nozzle, downstream of $X = 4$ m. The collector has a much smaller effect for the small nozzle configuration because the smaller jet interacts more weakly with the collector. The axial static pressure distribution shape is very consistent across wind speeds, which contributes to consistent drag coefficient measurements.

Comparison of the ASPD measured in the HALO wind tunnel with contemporary automotive wind tunnels is presented in Figure 32. The published data for the other wind tunnels is generally for a 140 km/h wind speed [9, 10, 14, 15, 16, 18, 19, 21].

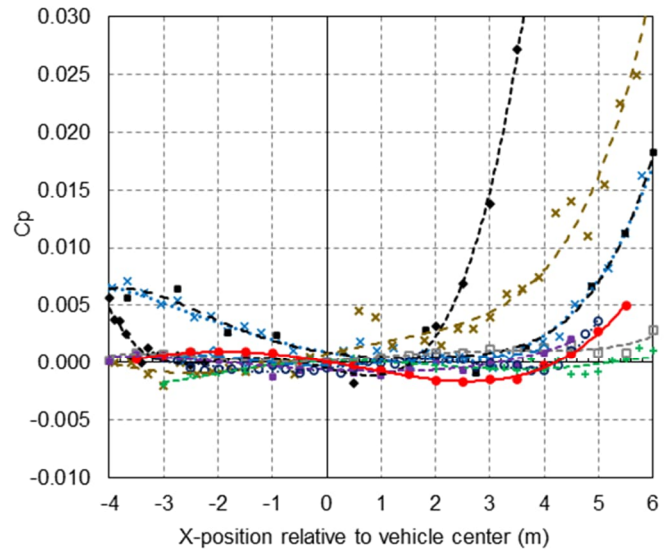


Figure 32. Axial static pressure distribution of several automotive aerodynamic and aeroacoustic wind tunnels.

Boundary Layer

A pickle fork probe was mounted on the forward-swept strut, which was attached to the flow survey traverse, as seen in Figure 33. The probe measured total pressure at a point above the moving ground plane, and static pressure was simultaneously measured 37 mm above this point.

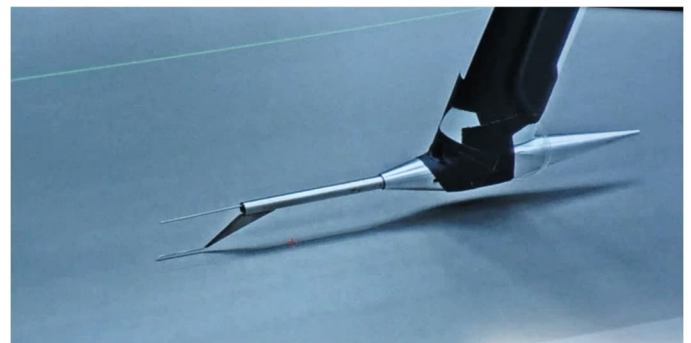


Figure 33. Pickle fork mounted on a forward-swept strut at the base of the flow survey traverse. The pitot tube is shown 2 mm above the moving belt.

Boundary layer measurements were made with both the 5-belt and single belt MGP systems for each nozzle size. The boundary layer profiles at multiple lateral positions for the small nozzle and single belt configuration is shown in Figure 34.

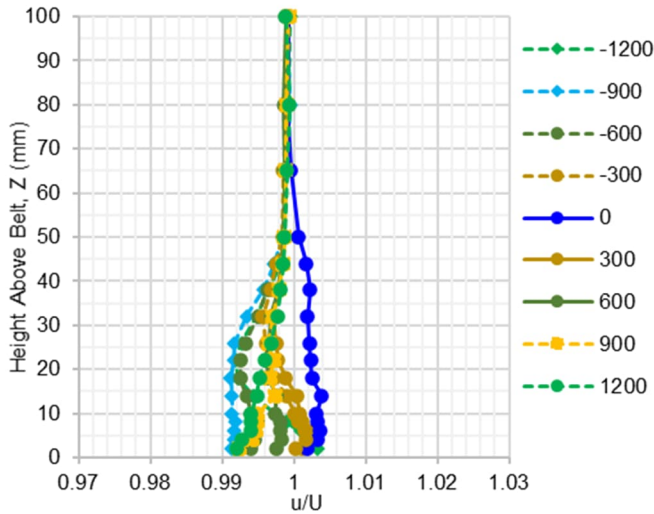


Figure 34. Boundary layer profiles at 300 km/h with the small nozzle, showing lateral uniformity over the single belt module. The data series are labelled according to the lateral (Y) position relative to centerline, in mm.

The objective having high lateral uniformity of the boundary layer was achieved using the primary scoop in the nozzle and the secondary suction/blowing slot just upstream of the moving belt. The adjustable loss plate across the span of the blowing slot allowed fine tuning of the boundary layer profile. The boundary layer profiles lie within a $\pm 1\%$ band at all measured speeds with the single belt, and this contributes to accurate simulation for front spoiler and underbody flow investigations. The same $\pm 1\%$ band was achieved over the center belt of the 5-belt moving ground plane, but this was of course over a narrower span, with $|Y| \leq 370$ mm.

The boundary layer displacement thickness at the upstream wheel drive units was measured to be less than 5 mm at all speeds.

Dynamic Pressure Uniformity

Measurements were done on three axial planes ($X = -2.5$ m, 0 m, and $+2.5$ m) relative to vehicle center. The measurement grid at each plane included 77 points for the large nozzle and 54 points for the small nozzle. The boundary layer control systems were functioning in automatic mode, and the moving ground plane speed was set to match wind speed.

Statistical analysis of the data showed maximum 1σ standard deviation of dynamic pressure of 0.24% and 0.16% for large and small nozzles, respectively, across all measured wind speeds. Figure 35 shows a contour plot of the dynamic pressure coefficient for the large nozzle for wind speeds of 180 km/h at $X = 0$.

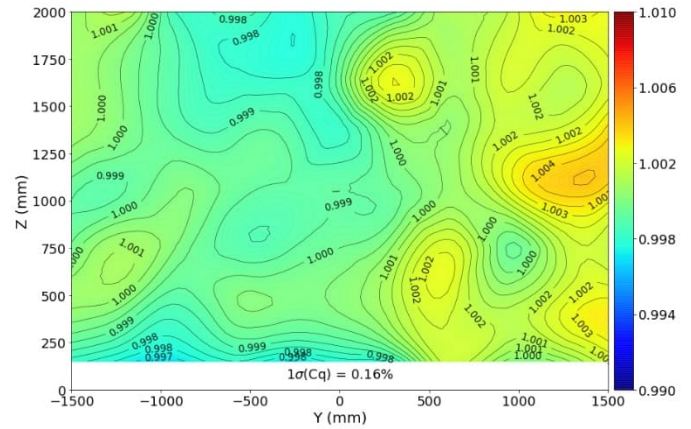


Figure 35. Dynamic pressure uniformity with the large nozzle at 180 km/h on a plane at $X = 0$ (vehicle center).

Flow Angularity

Flow angularity measurements were made with a CEA yawmeter probe, as seen in Figure 36. The flow angle probe was calibrated for each wind speed used for the flow angularity acceptance tests. Flow angularity was measured on planes at $X = -2.5$ m and $X = 0$ m.

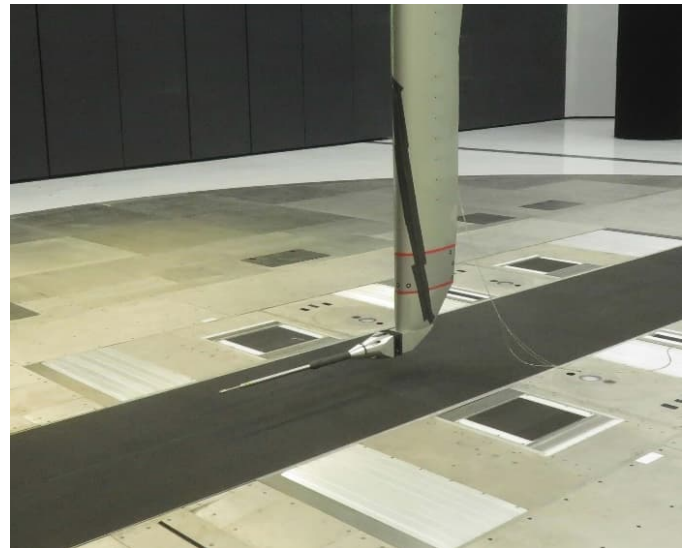


Figure 36. CEA yawmeter probe mounted on the flow survey traverse above the center belt of the 5-belt MGP.

The average flow angle for both pitch and yaw for each plane is less than $\pm 0.08^\circ$ for the large nozzle and less than $\pm 0.13^\circ$ for the small nozzle. Figure 37 is a flow angularity quiver plot on a plane at $X = 0$ with the large nozzle at 180 km/h. The plot includes calculated average and standard deviation of pitch and yaw.

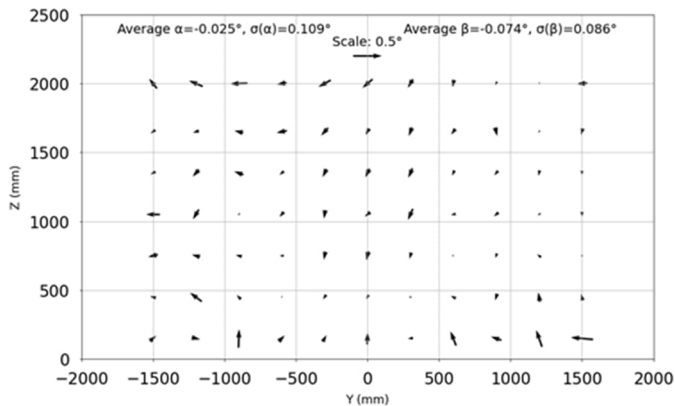


Figure 37. Flow angularity with the large nozzle at 180 km/h on a plane at X = 0.

Turbulence Intensity

Turbulence intensity measurements were made with a crosswire hot film probe. The bandpass used for the calculated turbulence results is 10 Hz to 5 kHz to remove the effects of velocity modulations inherent in open jets. The interaction between turbulence, open jet velocity steadiness, and low-frequency pressure fluctuations has been analyzed and discussed in [6].

Turbulence measurements were made in large and small nozzles on the X = -2.5 m plane and wind speeds. Overall results are listed in Tables 4 and 5. The large nozzle exhibited higher peak turbulence values, and these points occurred directly over non-moving portions of the 5-belt moving ground plane. The tests for the small nozzle were performed with the single belt moving ground plane and did not exhibit similar peaks. Turbulence intensity results were measured to be very low, with the maximum value at any speed of 0.17%, and average turbulence levels of 0.06% or lower. The turbulence intensity contour plot is presented for wind speed of 180 km/h large nozzle configuration in Figure 38.

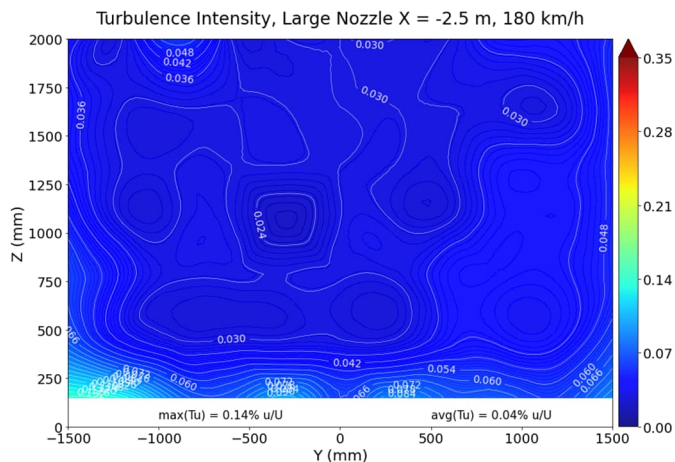


Figure 38. Turbulence intensity with the large nozzle at 180 km/h on a plane at X = -2.5 m.

Temperature Uniformity

The temperature uniformity test utilized an RTD probe mounted to the flow survey traverse. Detailed results are listed in Table 6. Figure

39 shows the temperature distribution as measured at 20 °C and 140 km/h in the large nozzle configuration.

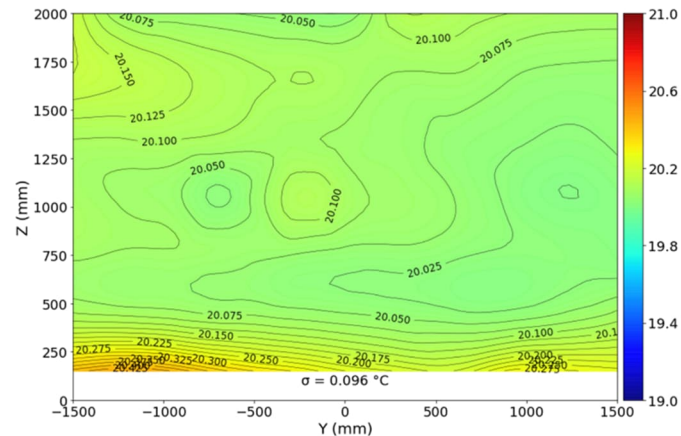


Figure 39. Air temperature uniformity with the large nozzle at 20 °C and 140 km/h on a plane at X = -2.5 m.

The temperature uniformity within the flow is excellent, with the only significant feature being a thermal boundary layer near the ground plane. This local gradient would diminish with extended soak times, although consideration must be given to testing productivity.

Summary and Conclusions

The HALO wind tunnel brings together a broad set of state-of-the-art testing capabilities into a single facility. The facility can be rapidly reconfigured between aerodynamic and acoustic testing modes for passenger vehicles and for motorsports vehicles, via a change of flex nozzle positions and swapping moving ground plane systems. Along with this functionality, the wind tunnel achieves parity with the best-in-class aerodynamics and acoustics performance.

The HALO wind tunnel introduces a range of new features that have contributed to functionality and performance.

- A new collector design optimized for acoustics, pulsation mitigation, as well as static pressure distribution.
- The anti-resonant plenum shaping eliminates one of the pulsation modes entirely.
- The primary boundary layer removal scoop can be seamlessly closed off in seconds by raising a section of flex floor for acoustic testing.
- The secondary boundary layer system allowed precise tuning of the boundary layer shape across the width of the moving ground plane.

Computational fluid dynamics and 1:8 scale testing supported the design development of the HALO wind tunnel, especially in the areas of acoustics, pulsation mitigation, and axial static pressure distribution.

The HALO wind tunnel's unique set of test capabilities enables Honda to advance the state of the art in passenger vehicle design for fuel economy and driving range, vehicle handling characteristics, and low cabin noise. Uncompromising motorsports testing is offered within the same facility, maximizing the utility of Honda's investment.

References

1. Mercker, E., Copper, K., "A Two-Measurement Correction for the Effects of a Pressure Gradient on Automotive, Open-Jet, Wind Tunnel Measurements," SAE Technical Paper 2006-01-0568, 2006, doi:[10.4271/2006-01-0568](https://doi.org/10.4271/2006-01-0568). The authors provided errata at the 2006 SAE Congress, which did not appear in the proceedings. A summary of the method (with corrections) is provided by Walter et al., SAE Technical Paper 2012-01-0300, doi:[10.4271/2012-01-0300](https://doi.org/10.4271/2012-01-0300).
2. Nishimura, M., Kudo, T., Nishioka, M., "Aerodynamic Noise Reducing Techniques by Using Pile-Fabrics," AIAA Technical Paper AIAA-99-1847, 1999, doi:[10.2514/6.1999-1847](https://doi.org/10.2514/6.1999-1847).
3. Best, S. and Zurich, J., "Lockheed Martin Low Speed Wind Tunnel Acoustic Upgrade," SAE Technical Paper 2018-01-0749, 2018, doi:[10.4271/2018-01-0749](https://doi.org/10.4271/2018-01-0749).
4. Allen, R., Gibbs, R., and Clark, P., "Flow-Induced Noise from Wind Tunnel Turbulence Reduction Screens," AIAA Paper 87-2728, 1987, doi:[10.2514/6.1987-2728](https://doi.org/10.2514/6.1987-2728).
5. Rennie, M., Kim, M.-S., Lee, J.-H., Kee, J.D., "Suppression of Open-Jet Fluctuations in the Hyundai Aeroacoustic Wind Tunnel", SAE Technical Paper 2004-01-0803, 2004, doi:[10.4271/2004-01-0803](https://doi.org/10.4271/2004-01-0803).
6. Arnette, S.A., Buchanan, T.D., Zabat, M., "On Low-Frequency Pressure Pulsations and Static Pressure Distribution in Open Jet Automotive Wind Tunnels", SAE Technical Paper 1999-01-0813, 1999, doi:[10.4271/1999-01-0813](https://doi.org/10.4271/1999-01-0813).
7. Wickern, G., von Heesen, W., and Wallman, S., "Wind Tunnel Pulsations and their Active Suppression," SAE Technical Paper 2000-01-0869, 2000, doi:[10.4271/2000-01-0869](https://doi.org/10.4271/2000-01-0869).
8. Rennie, M., "Effect of Jet Length on Pressure Fluctuations in ¾ Open Jet Wind Tunnels", Motor Industry Research Association (MIRA) Vehicle Aerodynamics Symposium, October 2000.
9. Nagle, P., Brooker, T., Bari, G., Toth, J., Skinner, S., "The Ford Rolling Road Wind Tunnel," SAE Technical Paper 2023-1-0654, 2023, doi:[10.4271/2023-01-0654](https://doi.org/10.4271/2023-01-0654).
10. Duell, E., Kharazi, A., Muller, S., Ebeling, W., and Mercker, E., "The BMW AVZ Wind Tunnel Center," SAE Technical Paper 2010-01-0118, 2010, doi:[10.4271/2010-01-0118](https://doi.org/10.4271/2010-01-0118).
11. Kharazi, A., Duell, E., and Walter, J., "Application of Helmholtz Resonators in Open Jet Wind Tunnels," SAE Int. J. Passeng. Cars - Mech. Syst. 6(1):436-447, 2013, doi:[10.4271/2013-01-1349](https://doi.org/10.4271/2013-01-1349).
12. Surface Vehicle Recommended Practice, SAE Technical Standard J1594, 2010
13. Waudby-Smith, P., Bender, T., and Vigneron, R., "The GIE S2A Full-Scale Aero-acoustic Wind Tunnel," SAE Technical Paper 2004-01-0808, 2004, doi:[10.4271/2004-01-0808](https://doi.org/10.4271/2004-01-0808).
14. Walter, J., Duell, E., Martindale, B., Arnette, S., et al., "The Driveability Test Facility Wind Tunnel No. 8," SAE Technical Paper 2002-01-0252, 2002, doi:[10.4271/2002-01-0252](https://doi.org/10.4271/2002-01-0252).
15. Walter, J., Duell, E., Martindale, B., Arnette, S., et al., "The DaimlerChrysler Full-Scale Aeroacoustic Wind Tunnel," SAE Technical Paper 2003-01-0426, 2003, doi:[10.4271/2003-01-0426](https://doi.org/10.4271/2003-01-0426).
16. Tadakuma, K., Sugiyama, T., and Maeda, K., "Development of Full-Scale Wind Tunnel for Enhancement of Vehicle Aerodynamic and Aero-Acoustic Performance," SAE Technical Paper 2014-01-0598, 2014, doi:[10.4271/2014-01-0598](https://doi.org/10.4271/2014-01-0598).
17. "Aero in the East", Wind Tunnel International, pp. 56-58, 2010.
18. Wickern, G. and Lindener, N., "The Audi Aeroacoustic Wind Tunnel: Final Design and First Operational Experience," SAE Technical Paper 2000-01-0868, 2000, doi:[10.4271/2000-01-0868](https://doi.org/10.4271/2000-01-0868).

19. Stumpf, H., et al., "The New Aerodynamic and Aeroacoustic Wind Tunnel of the Porsche AG," Springer Fachmedien Wiesbaden, 2015, doi:[10.1007/978-3-658-08844-6_54](https://doi.org/10.1007/978-3-658-08844-6_54).
20. Buckisch, R., Tokuno, H., and Knoche, H., "The New Daimler Automotive Wind Tunnel: Acoustic Properties and Measurement System," 10th FKFS Conference on Progress in Vehicle Aerodynamics and Thermal Management, Stuttgart, 2015.
21. Schwartekopp, B., "The New Daimler Automotive Wind Tunnel: Design and Aerodynamic Features," 10th FKFS Conference on Progress in Vehicle Aerodynamics and Thermal Management, Stuttgart, 2015.

Contact Information

Scott Best may be reached at Jacobs: scott.best@jacobs.com

Acknowledgments

The authors would like to acknowledge the support of the Honda team during the wind tunnel design and build project and for contributions to this paper. This included Thomas Ramsay, Mike Unger, Sam McCrary, Antonello Bianco, Matt Metka, Jim Przeklasa, and Jim McKillen. We also thank members of wind tunnel design team. Project management included Mike Barnes and Jay Whiteford. The aerodynamic design, commissioning, and acceptance team included Tyler McElroy, Tony Nagle, Ching-Wen Kuo, Martin Karanikolov, Bill Martindale, Joseph Yen, and Amir Kharazi. Ron Lipinski, Ravi Muthiah, Chris Wang, Matt Miller, Keith Swanson, and Michael VanHoose lead wind tunnel engineering and design teams. Tracy Tuck and Chris Walton were responsible for construction management.

Definitions/Abbreviations

ASPD	axial static pressure distribution
ATS	acoustic test systems
BLRS	boundary layer removal system
C_DA	vehicle equivalent drag area
CFD	computational fluid dynamics
C_pRMS	low-frequency pressure fluctuation root mean square normalized by free-stream dynamic pressure
C_q	dynamic pressure at a given point normalized by free-stream dynamic pressure
DES	detached eddy simulation
DLEX	diffuser leading edge extension
FOD	foreign object debris
HALO	Honda Automotive Laboratories of Ohio
MAU	make-up air unit
MGP	moving ground plane
OASPL	overall sound pressure level
OOF	out of flow (position)
RANS	Reynolds-averaged Navier Stokes
RTD	resistance temperature detector
STC	sound transmission class
T_{DP}	dew point temperature